INSTITUT FÜR AERODYNAMIK
UND GASDYNAMIK

Direktor: Prof. Dr.-Ing. F. X. Wortmann + kommiss.Leiter:Prof.Dr.-Ing.K.Förster
UNIVERSITÄT STUTTGART · PFAFFENWALDRING 21 · 7000 STUTTGART 80 (VAIHINGEN)

Telefon: (0711) 6851; Durchwahl: 685.....

Recent Wind Tunnel Experiments at Low Reynoldsnumbers

D.Althaus*

presented at the International Conference "Aerodynamics at Low Reynoldsnumbers $10^4 < Re < 10^6$ ", London, October 1986

This report on work at low Reynoldsnumber aerodynamics at the Institute for Aerodynamics and Gasdynamics of the University of Stuttgart may not begin without remembering the late Prof.Dr.F.X.Wortmann, who died in January 1985. In 1955 he started with his activities in this field. The author had the pleasure to work together with him almost from the early beginning. The well known FX-airfoil profiles are a result of this research. These profiles are used in general aviation, sailplanes, micro-lights, man-powered aircrafts (see the Musculair) R.P.V.'s and model-airplanes. A part of these airfoils are published in various papers and a catalogue /1/.

Laminarwindtunnel

The Laminarwindtunnel, constructed during the years 1958 to 1960 /2/ is a special design for twodimensional testing of airfoils and investigations of all problems associated with laminar flow at a very low turbulence level. It is an open return tunnel of the Eiffeltype with the high contraction ratio of 100 : 1, a rectangular 0,73 m * 2,73 m test section. Test-Reynolds-numbers are between $0{,}3 \cdot 10^6$ and $6 \cdot 10^6$. Fig.1 shows the overview of the tunnel, technical details are listed in Table 1. Fig.2 is a look downstream through the test section with an airfoil--model installed. The lift of a twodimensional airfoil is ascertained from the pressure distributions on the tunnel walls,

* Institut für Aerodynamik und Gasdynamik der Universität Stuttgart

the drag is ascertained from the total pressure loss in the wake by a rake which can be traversed through the test section and rotated in the direction of the flow. The moment of the airfoil is measured by a balance. A force balance for measuring lift and drag is also available. A PDP 11/34-Computer is used for experiment control and data acquisition. The corrected aerodynamic coefficients are plotted on line immediately by a digital plotter. Fig.3 shows a part of the instrumentation with the test-section in the background.

Modelwindtunnel

For airfoil tests at Reynoldsnumbers below $0,3 \cdot 10^6$ a smaller version of the Laminarwindtunnel was constructed and refined several times during the last years. It is also an open return tunnel with a rectangular test section with dimensions 0,37 m * 0,6 m, a contraction ratio of 19,6 : 1 and a turbulence level lower than $0,75 \cdot 10^{-3}$. Fig. 4 shows the Modelwindtunnel within the large laboratory hall of the Institute.

The models have a span of 0,37 m. Chord lengths from 100 mm to 200 mm enable test Reynoldsnumbers between 40 000 and 350 000. As in the large Laminarwindtunnel drag and moment are measured by a wake rake and a balance respectively, the lift is measured by a force balance.

The instrumentation was refined several times in the scope of student-courseworks. Fig.5 shows the test section with the arm of the lift balance and the momentum balance. Flow direction is from right to left. The wake rake is behind the trailing edge of the dark airfoil which is mounted horizontal. Fig.6 is a look on the instrumentation. Data processing and experiment control are now accomplished by a Commodore 8296 Computer coupled with an a/d-converter and relais output. Technical details are listed in Table 1. Test results of a series of airfoils are published in /3/ and /4/. It is well known that the environment as turbulence level, noise, vibrations have large influence on the test results

of windtunnels. Both tunnels were especially designed with these factors in mind.

In both tunnels airfoil drag is determined by rakes which can be traversed in the wake of the airfoil. When measuring drag by a force balance the interference effects between the airfoil and the tunnel walls deliver additional drag which is growing with incidence when compared to the drag measured by the wake rake. This is due to the interference of the model boundary layer with the turbulent wall boundary layers and due to airflow through the gaps between the model and the tunnel walls. This interference could be partly avoided by the use of three piece models where only the mid-span part of the model is fixed to the balance /5/. In this case only the interference of the gaps between the model parts can influence the measured drag. In order to get an idea about the magnitude of this additional drag an airfoil model consisting of two parts divided by a variable gap in the mid-span was tested in the Modelwindtunnel. By moving the wake rake along the span the integral of the total pressure loss in the wake was evaluated at many spanwise positions. Fig.7 shows the results for the symmetrical Eppler airfoil E 168 with a gap of 0,5 mm width at three incidences. In the position behind the gap a maximum in pressure loss exists followed by several periodic variations which are due to longitudinal vortices. At 9° angle of attack these vortices extend nearly to 100 mm span for the model with 160 mm chord. The additional drag caused by the gap ranges from 5% at α = 3° to 12% at α = 9° based on a model span of 250 mm, at a Reynoldsnumber of 200 000. On a three piece model two gaps exist but the middle part is influenced only by halve the additional drag of each gap. The result of this test may so be representative for the three-piece case. Knowing that the rake method has its disadvantages too it is prefered as it does not afford so complicated model construction.

In contrast to high Reynoldsnumber aerodynamics where great efforts are made to keep the flow laminar the problem at low Reynoldsnumbers is to achieve transition to turbulence early enough to avoid laminar separation without reattachment and to keep the laminar separation bubbles, which degrade the performance of the airfoil, as small as possible. This can be primarily achieved by the selection of suited velocity distributions or the boundary layer can be destabilized artificially.

In laminar separation bubbles the flow can be easily visualized by introduction of smoke. In Fig.8 smoke is emerging from the small tube resting on the model surface in the rear part of the model. Flow direction is from left to right, the bright line marks the model contour. The smoke fills a separated laminar boundary layer and shows a beginning of turbulence. The separated region extends downstream into the wake. This flow is said to be subcritical. In Fig.9 the smoke tube is within a laminar separation bubble which is formed by reattachment of the separated shear layer. The flow now is supercritical. On both figures the contour of the separating streamline is clearly visible. This method can be used to find the separation angle of the streamline.

Smoke wires are widely used to show the flow around airfoils when they are placed in front of the model /6/. In Fig.10 a smoke wire is placed parallel to the surface within a laminar separation bubble. Flow direction is from left to right, the dark area marks the model upper surface. The smoke moving against main flow direction clearly marks the laminar separation bubble. Owing to the very small velocities within the bubble the wire-Reynoldsnumber is not critical. By suitable positioning of the smoke wire within the bubble its contour can be explored. Both these methods of smoke visualization together with a video-camera are valuable tools for getting a quick look on the flow mechanism. Further simple devices used are a stethoscope to find the onset of turbulence within the bubble and the borders of the turbulent shear layer thus revealing the reattachment of the layer and a down of a goose

feather fixed to a thin wire by which backflow in separated regions can be detected. These methods were used in the low Reynoldsnumber tests described in the following.

Hysteresis

A specific characteristic of airfoils at low Reynoldsnumbers which occurs sometimes is the hysteresis in lift and drag. The coefficients of both form a loop between increasing and decreasing incidence. Some airfoils are reported to have clockwise, others to have counterclockwise hysteresis loops. In order to get more insight into the mechanism of these effects the flow on several airfoils was studied in the Modelwindtunnel.

As the hysteresis of lift and drag are coupled with one another lift hysteresis was explored primarily. To ascertain the lift coefficient in its dependence from incidence and Reynoldsnumber analog devices were used. In a divider the signal from the lift balance was divided by a signal of a pressure transducer measuring dynamic head thus rendering a voltage proportional to lift coefficient. With another voltage proportional to incidence the lift coefficient c_L could be plotted over angle of attack α immediately on an analog x,y-plotter. Another analog device formed the square root of the signal proportional to the dynamic head. The airfoil incidence is actuated by an electric motor with variable constant velocity. Thus the lift coefficient could be plotted over the Reynoldsnumber on a second analog plotter. By these devices c_L vs. α or c_L vs. Re diagrams easily can be plotted by very slowly changing the angle of attack of the tunnel velocity.

FX 63-137 airfoil /1,3,10/

This airfoil has a high zero-lift owing to its rather high camber. It was initially designed for Reynoldsnumbers greater 0,5 million but it is often used at lower Reynoldsnumbers now. Fig.11 shows its theoretical velocity distribution for various angles of attack. In Fig.12 the lift coefficient c_L is plotted over the incidence α.

Note: On this and all following c_L plotts demonstrating hysteresis loops the c_L values are not exactly to scale as only their variation with α or Re, not their absolute values are of interest. The interpretations of the flow mechanism following are results of many flow visualization studies described above.

At the Reynoldsnumber 80 000 the boundary layer at the upper side of the airfoil remains detached after laminar separation during the whole range of incidence. The flow is called to be subcritical. When the Reynoldsnumber is raised only to 85 000 a quite different behaviour exhibits: The lift curve slope is higher from the very beginning. At an incidence of about 7 degrees the lift jumps up following a higher slope. At 20° there is a sharp stall. The lift curve then follows the subcritical slope. The same holds for decreasing incidence. At an incidence of 10° the lift goes up following the higher slope down to 5,5 degrees when it jumps down again to follow the initial curve. For this Reynoldsnumber the lift vs. α curve resembles a lying eight with a low and narrow counterclockwise and a wide high clockwise loop. At Re = 135 000 the lift curve slope is higher in general and nearly linear up to maximum lift. Stall is reached at an incidence 2° higher and recovery happens already when incidence is lowered to 14°.

As this types of flow mechanism were observed on several airfoils the tests on the FX 63-137 will be discussed in more details: Flow visualizations revealed that increase in lift at α = 7° is accompanied by the reattachment of the separated shear layer at the trailing edge: this is the transition from subcritical to the supercritical state. At decreasing incidence from stall the separated shear layer reattaches at the trailing edge when α = 10° forming a long separation bubble which separates again when the incidence is as low as $\approx$ 6°. At this Re-number instability of the separated shear layer is too low to provoke turbulence, only subcritical flow can exist.

On Fig.13 the subcritical-supercritical hysteresis loop is removed by a tripping device consisting of a 10 mm wide tape with digged-in bumps every 5 mm span, totalheight 0,4 mm. This "bump-tape" ended

at x/c = 40%. By this means the shear layer over the laminar separation bubble forming at about x/c = 40% (where the velocity gradient along the chord gets larger) is destabilized in a manner that subcritical flow is prevented at this Re-number.

Nearly the same behaviour could be achieved when the flow on the smooth airfoil was excited by sound with a frequency of 285 Hz and a sound pressure level of 80 dB. This is shown in Fig.14 for the same Re-number. The sound was radiated by a loudspeaker at the upper side of the test-section above the model surface. Sound pressure was measured at the place of the model.

Fig.15 shows the effect of a scotch tape with a height k = 0,12 mm giving $k/c = 0{,}8 \cdot 10^{-3}$ (c = 160 mm) and a width of w = 2 mm positioned at x/c = 1%. This tripping device affects the laminar separation bubble forming near the airfoil nose. At increasing incidence the lift falls nearly linear beyond $c_{L\ max}$ as the separation of the turbulent boundary layer moves forward. Bursting of the bubble is delayed by about three degrees compared to the smooth model. At decreasing incidence the lift begins to rise immediately the bubble begins to close lift is restored at the angle of attack of $c_{L\ max}$. At low incidences subcritical behaviour remains unaffected showing a small loop. Tripping the laminar separation bubble near the nose strongly reduces the high incidence loop. If the "bump-tape" as already used in Fig.13 is added the flow becomes again supercritical at low incidence without changes at high incidence.

In Fig.16 lift-drag polars demonstrate the effect of the tripping devices. The drag of the smooth airfoil at Re = 85 000 is in the range of the diagram only when the flow has become supercritical, while the polars with the tripping devices show a drastic improvement. Even at the higher Reynoldsnumber of 150 000 they render smaller drag coefficients than the smooth airfoil. For the airfoil with both tapes however the drag begins to rise at a lower lift.

Further experiments with excitation by sound showed that the subcritical-supercritical hysteresis loop can be removed by a relatively low intensity. At the high incidence loops however only their extension in α-direction could be diminished by the sound

power available. The higher the Reynoldsnumber the higher was the required sound power and frequency.

In Fig.17 the variation of lift coefficient with the Re-number is plotted. For the incidence $\alpha = 5°$ the lift of the smooth airfoil begins to increase slowly for Re above 80 000. By excitation with sound lift begins rising even below Re = 60 000. Both curves show no hysteresis. By tripping with the "bump-tape" lift begins to rise at about Re = 70 000. For this condition the lift shows a hysteresis when the Reynoldsnumber is lowered down about 50 000. At $\alpha = 10°$ incidence the rise of lift coefficient with Re-number is steeper, all cases show hysteresis effects due to the separation bubbles. For both angles of attack the curves level out for Re-numbers above 100 000. The Reynoldsnumber at which the lift begins to rise is called the critical Re-number.

In Fig.18 the lift coefficient is plotted against sound frequency at a constant sound pressure level of 80 dB and an incidence of 10°. The analog output of a frequency generator was connected to the x-axis of a x,y-plotter. For Re = 40 000 there is no reaction. At Re = 60 000 there is a steep rise in lift for f = 280 Hz, at f = 380 Hz it falls down again. When the frequency is decreased the lift rises at 280 Hz and stays high down to 260 Hz. At Re = 70 000 increasing frequency produces a maximum in lift at nearly 300 Hz, then the influence of sound decreases. At decreasing sound frequency there is no reaction on lift. At this Re-number the sound pressure of 80 dB was not high enough. There is a rather narrow band of effective frequencies and excitation seems to be more effective when the frequency is increased than when it is decreased.

The Lissaman 7768 and the Miley M06-13-128 airfoils are often cited when discussing hysteresis effects at low Reynoldsnumbers /7,8,9/. At the University of Notre Dame /7/ the Miley airfoil was found to have a counterclockwise hysteresis loop and the Lissaman airfoil to have a clockwise one. The theoretical velocity distributions for both are shown in Fig.19 and Fig.20. Both have nearly the same height in velocity peak at the upper side followed by a concave pressure rise.

The Lissaman has its peak at x/c = 30% while at the Miley airfoil the peak is at x/c = 40%, its pressure gradient to the trailing edge is higher therefore than of the Miley airfoil.

Lissaman 7669 airfoil

Fig.21 shows the lift versus incidence curves. For Re = 100 000 the flow is subcritical at all incidences tested. At moderate angles of attack laminar flow separation occurs at the beginning of the pressure rise and moves towards the leading edge with growing angle of attack. When the Reynoldsnumber is increased to 150 000 the lift curve shows hysteresis loops in form of a lying eight similar to the FX 63-137 airfoil (Fig.12). The flow is subcritical above $\alpha = 4°$. This is due to laminar separation without reattachment at the beginning of the concave pressure rise. At about $\alpha = 12°$ the separated shear layer attaches at the trailing edge, the flow gets supercritical, and the lift jumps up. Now laminar separation moves towards the leading edge. At the same time the separation bubble becomes shorter and the separation of the turbulent boundary layer moves upstream. The lift degrades until the bubble bursts at about 21°. At decreasing incidence the lift jumps up again when the short bubble reforms at about $\alpha = 13°$. This bubble grows in length until at $\alpha = 8°$ the flow is subcritical again.

At Re = 200 000 the flow is supercritical from the beginning at low incidence and only the loop at high incidence appears. The same behaviour can be achieved at Re = 150 000 when the laminar separation bubble at the beginning of the pressure rise which is responsible for the lower loop is influenced by a tripping device. Fig.22 shows that a Mylar tape with a height k = 0,24 mm, $k/c = 1{,}4 \cdot 10^{-3}$ and a width of 3 mm fixed at x/c = 16% removes a lower loop. The lift now behaves just as in Fig.21 for the higher Re = 200 000.

c_L vs. α plots for the airfoil with the Mylar tape at x/c = 16% (Fig.23) show that the lower loop is removed now even for the low Re = 100 000. The remaining loop is getting narrow more and more with growing Reynoldsnumber. Fig.24 demonstrates the changes in drag caused by the tripping device: The c_L vs. c_D polars for the smooth airfoil show a drastic loss in drag in the c_L range of the lower hysteresis loop (Fig.21) at Re = 100 000 and 150 000. At Re = 225 000 where the flow is all supercritical the drag behaves well. By the Mylar tape as tripping device an enormous improvement in drag is obtained. Even at the low Re = 100 000 the drag stays low in the complete lift range. At Re = 150 000 the drag for the tripped airfoil is partly as low as for the smooth airfoil at the very higher Re = 225 000. This example shows that large improvements are possible by properly selected tripping devices. Test with excitation of the flow by sound gave similar results as at the FX 63-137 airfoil.

Test results of the Lissaman 7669 airfoil for Reynoldsnumbers between 0,7 and 2,5 millions from the Laminarwindtunnel are shown in Fig.25. It should be noted that the drag scale in this diagram is quite different.

Miley 06-13-128

The lift versus α behaviour for the smooth Miley airfoil is plotted in Fig.26. For Re = 80 000 the flow is subcritical in the entire range of incidence tested. At Re = 100 000 flow is subcritical up to the high incidence of 20° when lift jumps up as supercritical flow is achieved and a short bubble forms near the leading edge, bursting at 22°.

At decreasing incidence this bubble reattaches and expands in length downstream. Separation of the turbulent boundary layer moves towards the trailing edge, the lift increases. At the same time the reattachment point of the bubble moves downward too. With decreasing incidence the instability of the laminar boundary layer

at the separation point is reduced. Consequently transition in the separated shear layer is delayed until it can not reattach upstream of the trailing edge, the flow becomes subcritical and lift jumps down. At Re = 220 000 there is no subcritical range. The lift shows a narrow loop at high incidences. The c_L versus c_D polars in Fig.27 show a drastic penalty in drag for Re = 100 000 and 150 000 in the range of the lower hysteresis loop between c_L above 0,2 and below 1,3. Even at Re = 225 000 there is still an indenture in drag left. Fig.28 demonstrates that the double loop hysteresis can be avoided by a Mylar tape at x/c = 18%. By the addition of a Scotch tape at x/c = 1% the laminar separation bubble near the leading edge can be influenced thus avoiding hysteresis at all. This is payed off however by a loss in maximum lift. When the tripping device is fixed too far downstream (Fig.29) it is only partly efficient. It can not provoke supercritical flow at incidences between 8° and 13°.

Even at the low Reynoldsnumber 80 000 the flow is supercritical with the Mylar tape at x/c = 18% resulting in a broad upper loop (Fig.30), which can also be removed by an additional Scotch tape at x/c = 1% but with a loss in maximum lift. The c_L vs. c_D curves for the airfoil with the Mylar tape at x/c = 18% (Fig.31) show an enormous gain in drag remembering that at the smooth airfoil (Fig.27) flow was subcritical for Re = 100 000 and 150 000. At Re = 80 000 and 100 000 there is a small indenture left in the drag values but at Re = 150 000 drag is less than for Re = 225 000 at the smooth airfoil. Tests with excitation of the flow by sound gave similar results as at the FX 63-137 airfoil mentioned above.

AH 79-100 B /1/

In Fig.32 the theoretical velocity distribution for $\alpha = 0°$ shows the peak velocity at x/c = 30% followed by a gentle pressure rise down to x/c = 55% and a lightly concave distribution to the trailing edge. The lift versus α diagram (Fig.33) demonstrates a subcritical-supercritical double loop for Re = 60 000 and the supercritical loop for Re = 100 000.

E 214

At $\alpha = 0°$ the velocity peak of the theoretical velocity distribution of the Eppler airfoil (Fig.34) is at $x/c = 28\%$ followed by a gentle pressure rise with a transition to a steeper one at $x/c = 85\%$. The flow is subcritical at Re = 35 000 in the whole range of incidence. At Re = 40 000 a double loop hysteresis is observed, at Re = 60 000 only the high-lift loop is left. The drag reveals an indenture at this Reynoldsnumber (Fig.36).

Conclusions

From the examples presented it can be concluded that hysteresis at low Reynoldsnumbers is caused by two different mechanisms:

1. At the low angles of attack by transition from the subcritical to the supercritical state of flow and vice versa. Supercritical flow exists when a separated shear layer reattaches at the trailing edge forming a midchord bubble.
2. At high angles of attack by bursting and reattachment of a laminar separation bubble near the leading edge.

When both mechanisms are effective a double loop, forming a lying eight exists. The loops are not formed by two separated circles but are interlaced. High lift hysteresis is caused by the fact that a closed bubble can sustain a rather strong pressure rise until bursting. But for reattachment it needs far better conditions, i.e. a rather lowered incidence. The same holds for the low-lift hysteresis: Starting from an incidence near zero a rather high instability of the separated shear layer is needed to produce turbulence and close the long midchord bubble at the trailing edge. At decreasing incidence the closed bubble is resistent against bursting down to a lower angle of attack.

One reason that bubbles take longer to reform than to burst may be the fact that there is a feedback of turbulence within a closed bubble. This feedback is missing in a free shear layer. Double loop hysteresis can only appear where subcritical flow can exist. When looking at the theoretical velocity distributions of the airfoils

demonstrated here as examples, it can be concluded that as a characteristic feature all show a rather gentle pressure rise behind their velocity peaks which is followed by a bend to a steeper pressure gradient, this bend being stronger if it is followed by a concave pressure rise. Airfoils with velocity distributions of this type tend to have subcritical flow at low Reynoldsnumbers, and are mostly designed for higher Reynoldsnumbers. At low Reynoldsnumbers only airfoils with convex velocity distributions and gentle gradients without any bend should be used.

As was demonstrated subcritical flow on airfoils can be avoided by the use of suited tripping devices. By this means large improvements in performance in a certain range of Reynoldsnumbers can be achieved. Tripping devices must be carefully positioned in order to be efficient without a penalty.

Excitating the flow by sound renders the most possible improvements available since the flow is not disturbed by any device within the boundary layer. Frequency and sound pressure level must be adjusted however. Similar results as reported by other investigators /10/ were found. Unstalled flow could be brought to reattach by sound merely within the hysteresis loops. When the flow had reattached sound could be turned off without any effect. At low angles of attack subcritical flow can be made supercritical by sound, but it returns to the subcritical state when sound is turned off.

Excitation by sound and the use of tripping devices have similar effects as increasing the turbulence intensity of the flow.

Looking at Fig.36 the drag has a large indenture with lift coefficient at Re = 60 000 although the flow is supercritical. Starting from low lift coefficients a maximum in drag is reached at about $c_L = 0,8$ followed by a maximum at $c_L = 1,2$, which is only a small peak. This form of a lift-drag polar is characteristic for airfoils with a large laminar separation bubble near midchord of the upper surface. Beginning at moderate lift the bubble grows with the pressure gradient becoming steeper. This causes increasing drag. Above the maximum in drag at $c_L = 0,8$ the growing instability of the separated shear layer causes earlier transition within the bubble followed by

earlier reattachment. The drag coefficient decreases until transition within the bubble has moved up to the separation point. This means the bubble has vanished. This phenomenon is typical for many airfoils up to Reynoldsnumbers in the order of two millions. This drag penalty can also be overcome by the use of properly selected and positioned transition devices which destabilize the free shear layer thus causing earlier transition and reattachment. This principally has the same effect as increasing the Reynoldsnumber, the indenture in drag is removed. But it is impossible to achieve drag coefficients lower than the minimum drag peak at c_L = 1,2 where the laminar separation bubble just disappears and normal transition of the boundary layer takes place.

Transition devices have proved to be successful at many airfoils in a large range of Reynoldsnumbers.

Theoretical polars at low Reynoldsnumbers

The experimental results presented above demonstrate the complexity of low Reynoldsnumber flow. A complete theoretical treatment is not possible up to today. The design of airfoils is mostly a matter of experience and guess. At least at Reynoldsnumbers below 200 000 theoretical airfoil polars must be considered with caution. Two airfoils designed by M.S.Selig /8/ were tested in the Modelwindtunnel. The results are plotted in Fig.37 and Fig.38 together with the theoretical polars given by the designer. For the Selig S-3021 airfoil the theoretical (full lines) and experimental (dashed lines) lift-drag curves show rather small differences for Re = 200 000 but a rather large discrepancy for Re = 100 000. At the Selig S-2091 airfoil in Fig.38 the difference at Re = 100 000 is still larger. The experimental points for Re = 60 000 demonstrate that the flow is subcritical for c_L above 0,2.

Some experimental airfoil polars

Some airfoils which may be of interest for model airplanes were tested in the Modelwindtunnel during the last time. The results are presented without further comment:

Fig.39 : Selig S-3021-095-84
Fig.40 : Selig S-2091-101-83
Fig.41 : Eppler E 184 designed for tailless wings
Fig.42 : Eppler E 197
Fig.43 : Eppler E 205
Fig.44 : Eppler E 222
Fig.45 : Eppler E 226
Fig.46 : Eppler E 230

For comparison see /3,4/.

So far the results from the Modelwindtunnel. In the Laminarwindtunnel besides some industrial contracts a research program in laminar separation bubbles at Reynoldsnumbers between 0,7 and 3 millions is in progress. First results will be available during 1987.

References

/1/ D.Althaus und F.X.Wortmann : Stuttgarter Profilkatalog I
Friedr.Vieweg & Sohn Braunschweig, 1981

/2/ F.X.Wortmann und D.Althaus : Der Laminarwindkanal des Instituts für Aerodynamik und Gasdynamik an der Technischen Hochschule Stuttgart, Z.f.Flugwiss.12 (1964), pp 129-134.

Aircraft Research Association, A.R.A.Library Translation No.7, Manton Lane, Bedford,Aug. 1964.

/3/ D.Althaus : Profilpolaren für den Modellflug, Neckar-Verlag Villingen-Schwenningen 1980

/4/ D.Althaus : Profilpolaren für den Modellflug,Band 2 Neckar-Verlag Villingen-Schwenningen 1985

/5/ T.J.Mueller and B.J.Jansen : Aerodynamic Measurements at low Reynoldsnumbers. AIAA paper 82-0598, 1982

/6/ S.M.Batill and T.J.Mueller : Visualization of the Laminar-Turbulent Transition in the Flow over an Airfoil using the Smoke-Wire Technique. AIAA paper 80-0421,1980

/7/ T.J.Mueller : The Influence of Laminar Separation and Transition on Low Reynoldsnumber Hysteresis. AIAA paper 84-1617, 1984

/8/ M.S.Selig : The Design of Airfoils at Low Reynolds-numbers. SOARTECH III,c/o H.A.Stokely, 1504 Horseshoe Circle, Virginia Beach, Virginia, 23451, July 1984

/9/ M.S.Selig : Addendum to the Design of Airfoils at Low Reynoldsnumbers, SOARTECH IV, Jan.1985

/10/ V.Sumantran, Z.Sun, J.F.Marchman III: Acoustic and Turbulence Influence on Low Reynoldsnumber Wing Pressure Distributions. Proceedings of the Conference on Low Reynoldsnumber Airfoil Aerodynamics. Edited by T.J.Mueller UNDAS-CP-77B123, June 1985

Table 1 : Technical details of windtunnels

Laminarwindtunnel:

Main use : twodimensional tests of airfoil profiles

Reynoldsnumber : from $0,3 \cdot 10^6$ to $6 \cdot 10^6$ / meter model chord

Low turbulence level $< 1 \cdot 10^{-4}$

Contraction ratio : 100 : 1

Maximum flow velocity: 90 m/s

Fan : 8 blades, angle of attack adjustable at rest
Diameter: 2,7 m

$Rpm_{max} = 440$

Drive installation: 3-phase electric motor 180 kw
hydraulic coupling for adjustment of tunnel velocity

Area of filters at intake: 200 m²

Area of screens : 40 m²

Test section dimension : 2,73 m * 0,73 m = 2 m²
model span 0,73 m

Length of tunnel : 46 m

Modelwindtunnel:

Main use : twodimensional tests of airfoil profiles

Reynoldsnumber : from 40 000 to 350 000

Turbulence level : $0,75 \cdot 10^{-3}$

Contraction ratio : 19,6 : 1

Maximum flow velocity : 25 m/s

Drive installation : electric motor 0,75 kw
tunnel velocity adjustable by a continuously adjustable mechanical gear.

Fig.1 : Laminarwindtunnel

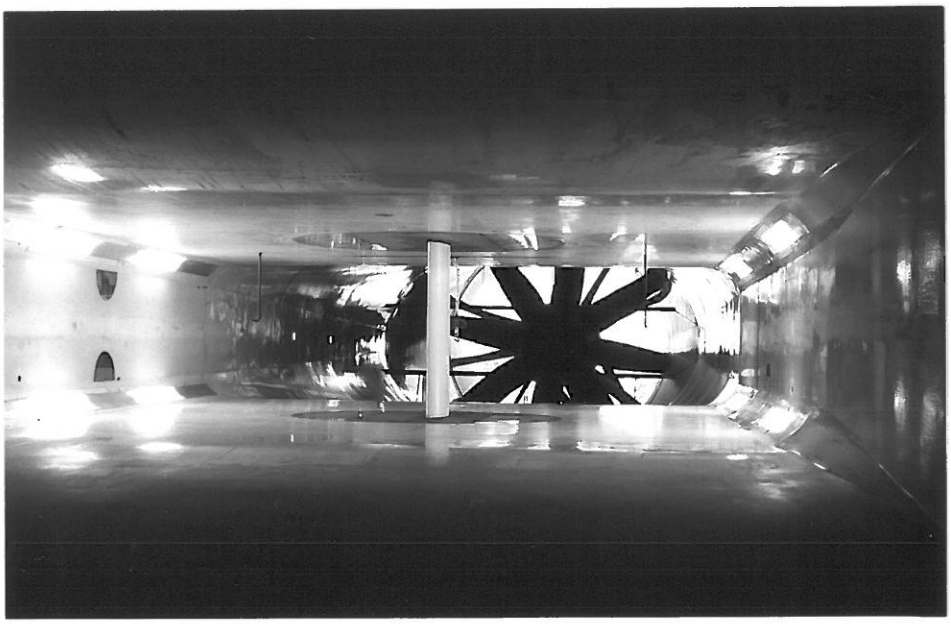

Fig.2 : Looking downstream through the test section of the Laminarwindtunnel

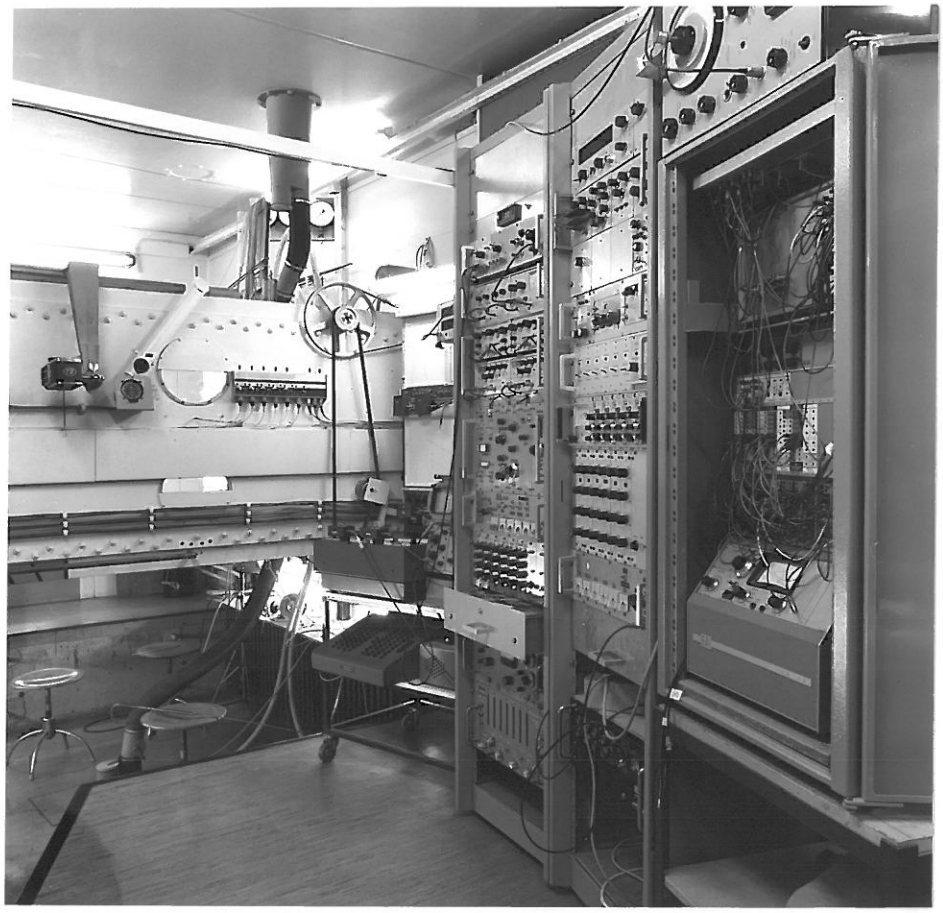

Fig.3 : Instrumentation of the Laminarwindtunnel with test section in background

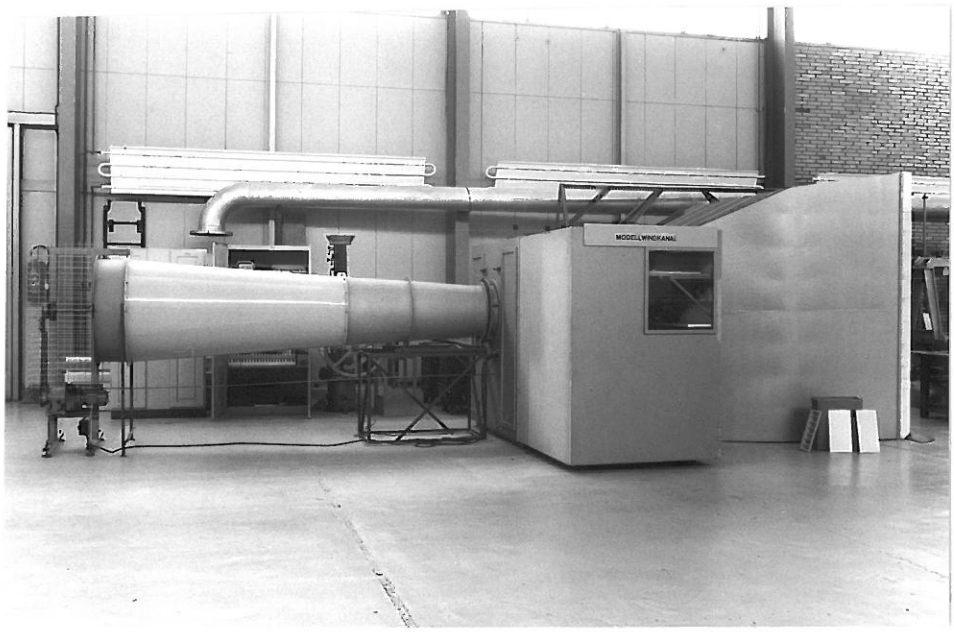

Fig.4 : Modelwindtunnel in the laboratory hall

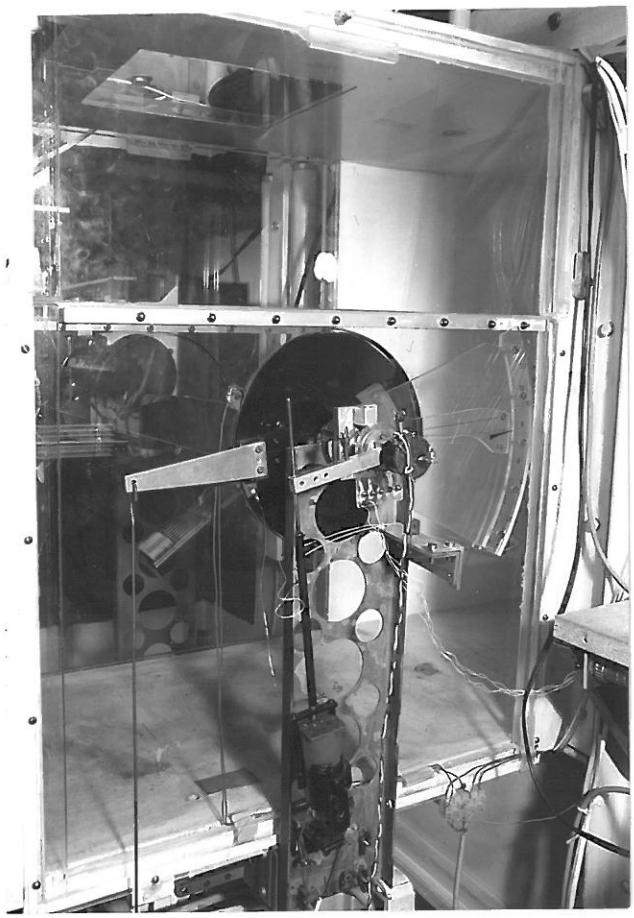

Fig.5 : Test section of the Modelwindtunnel
Flow direction is from right to left. The dark painted model is mounted horizontal.

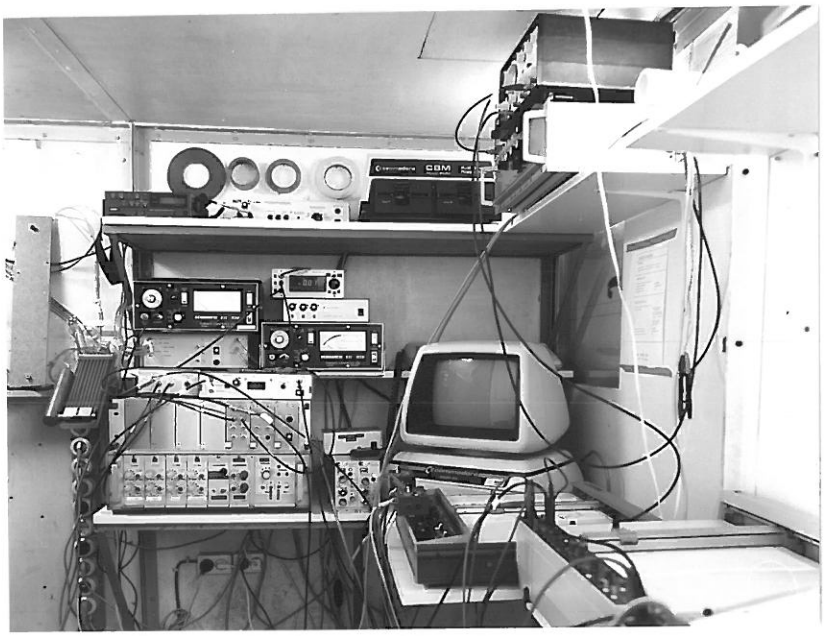

Fig.6 : Instrumentation of the Modelwindtunnel

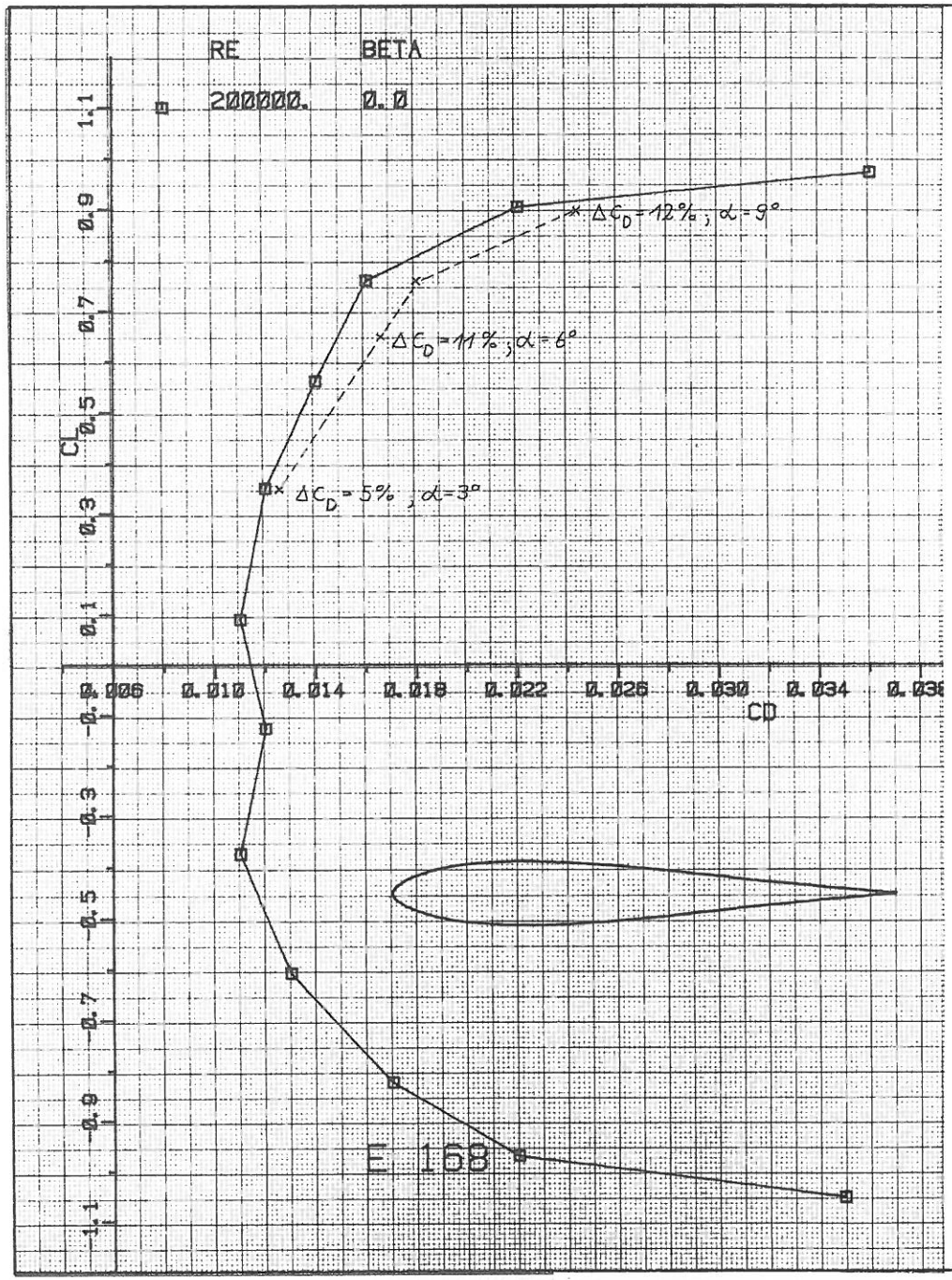

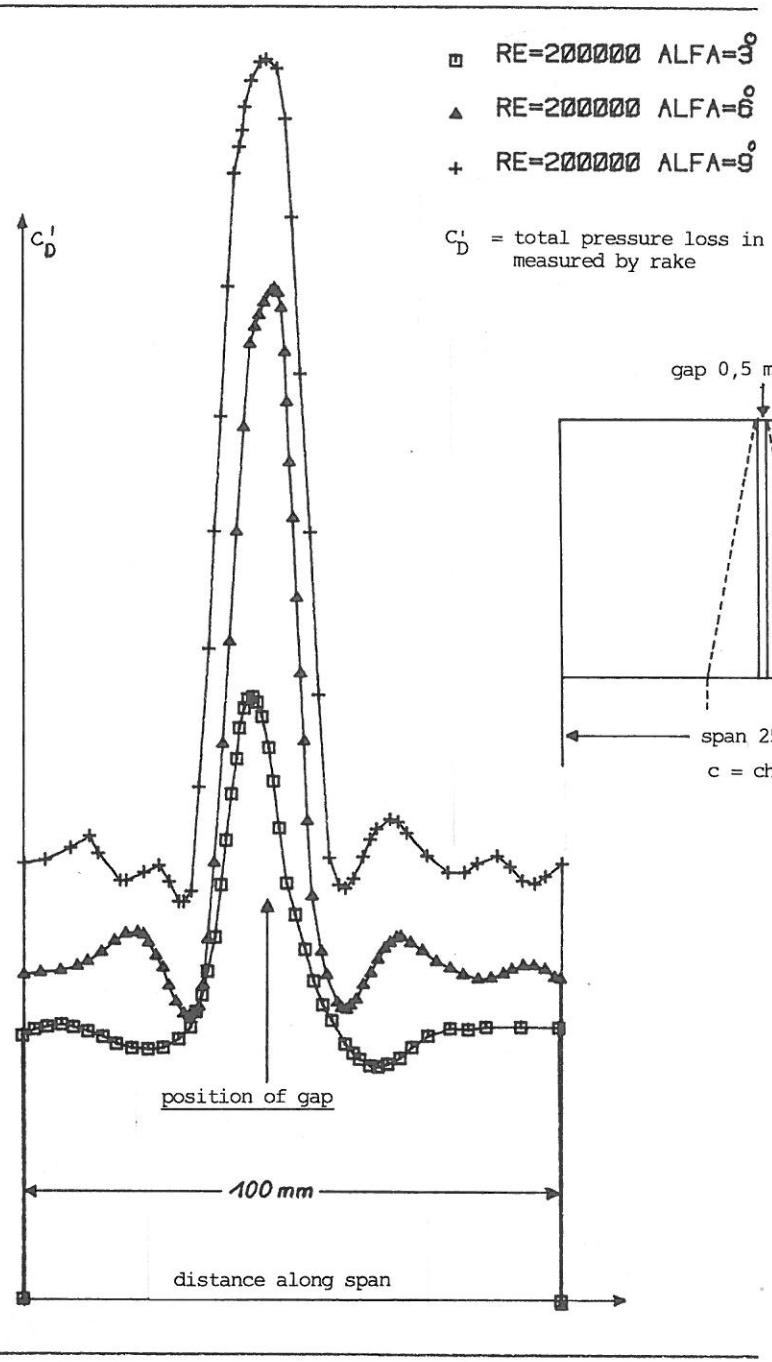

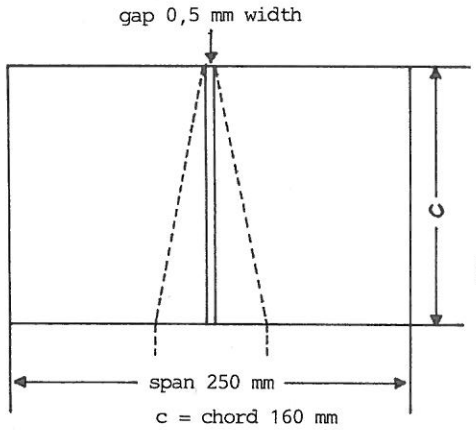

Fig.7 Drag increase due to gap in wind-tunnel-model

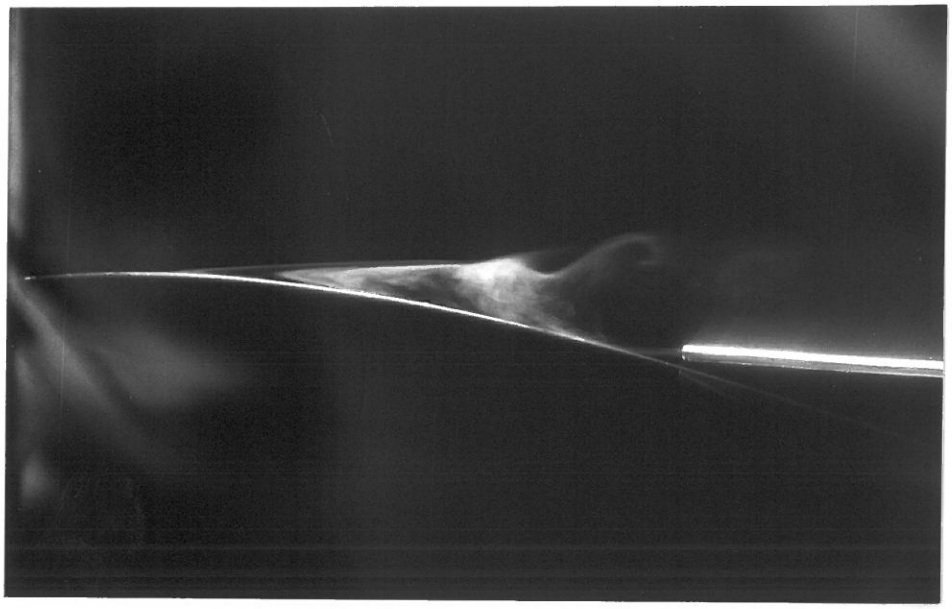

Fig.8 : Smoke in a separated laminar boundary layer without reattachment (subcritical flow). Flow direction is from left to right. Smoke is supported by the small tube at the right.

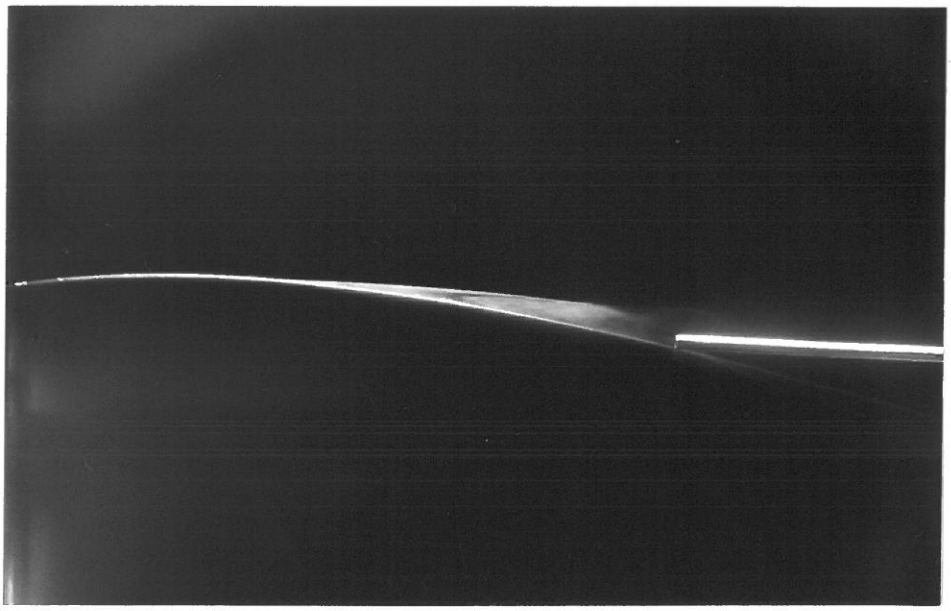

Fig.9 : Smoke in a laminar separation bubble

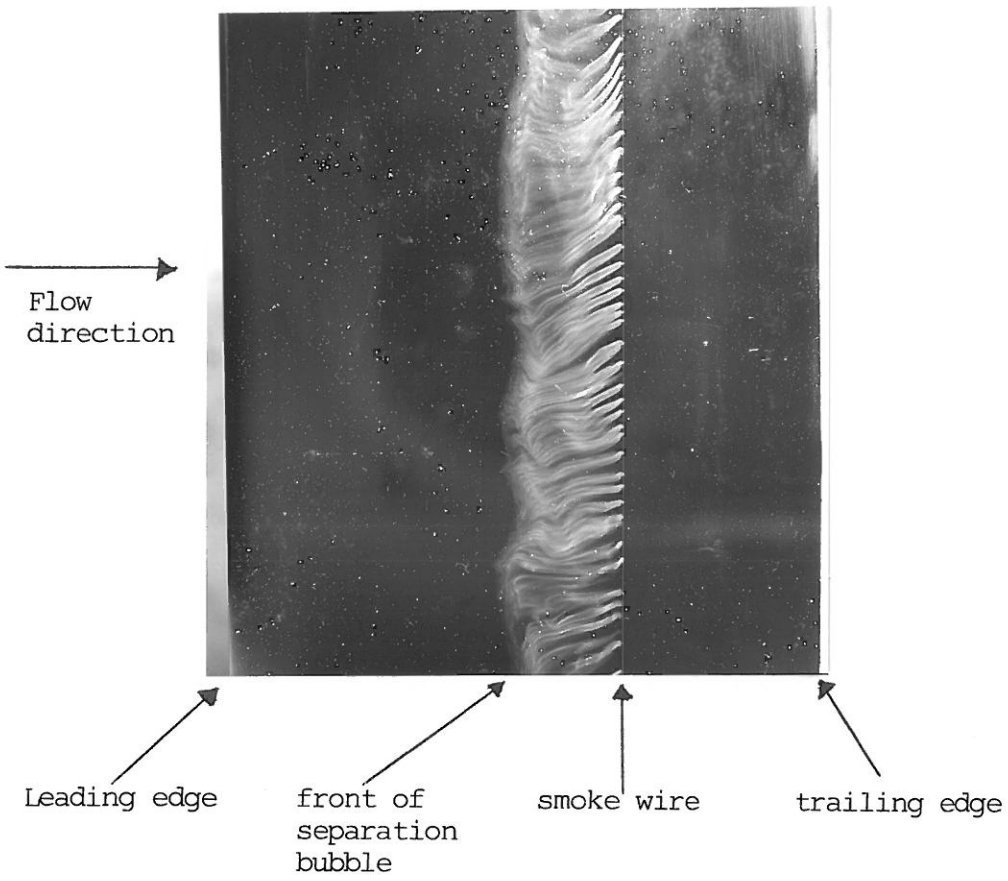

Fig.10 : Smoke wire parallel to the model surface within a laminar separation bubble. The smoke moves against the direction of flow which is from left to right. The dark area marks the model upper surface.

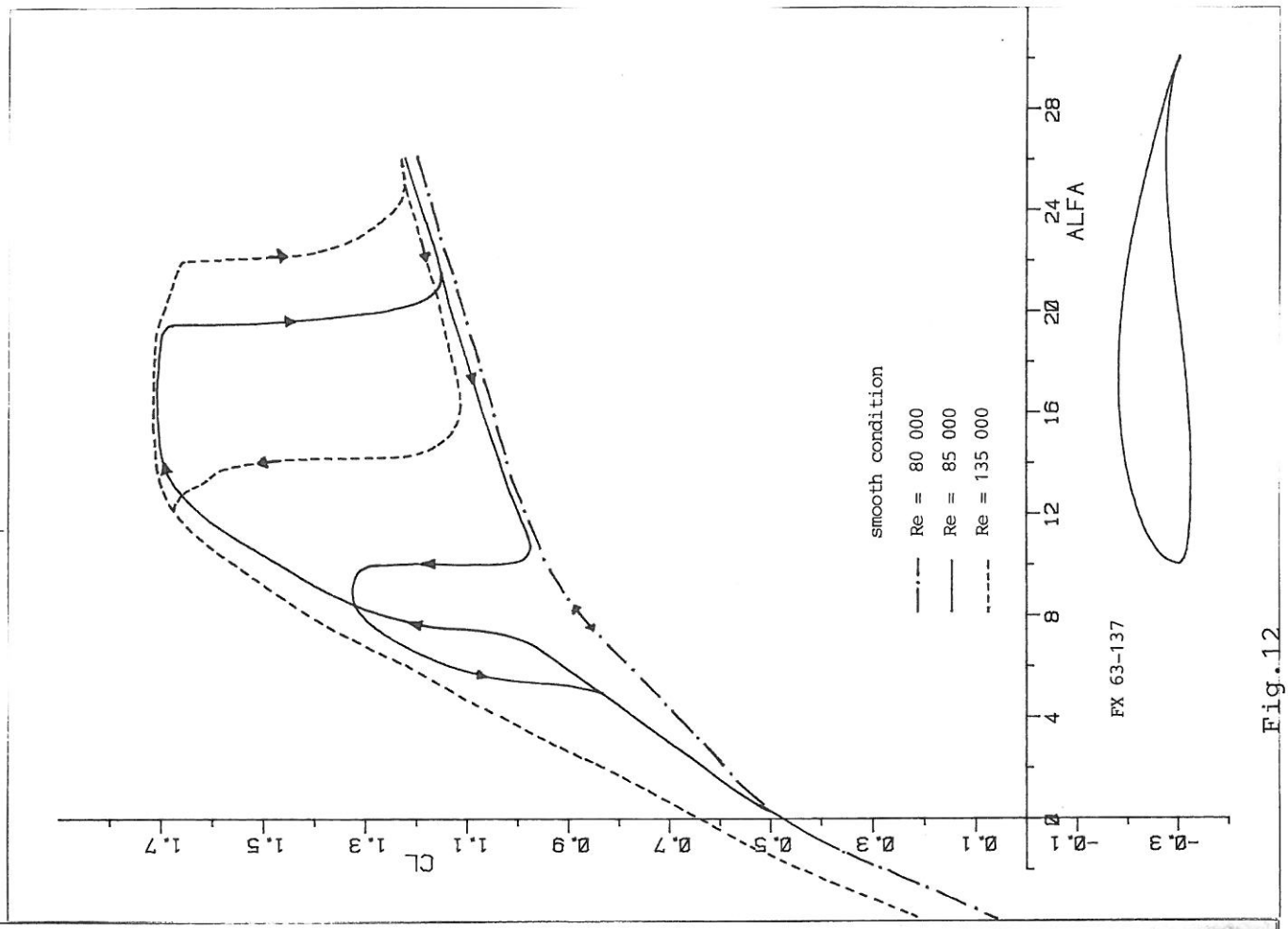
smooth condition
Re = 80 000
Re = 85 000
Re = 135 000
CL
ALFA
FX 63-137

Fig.12

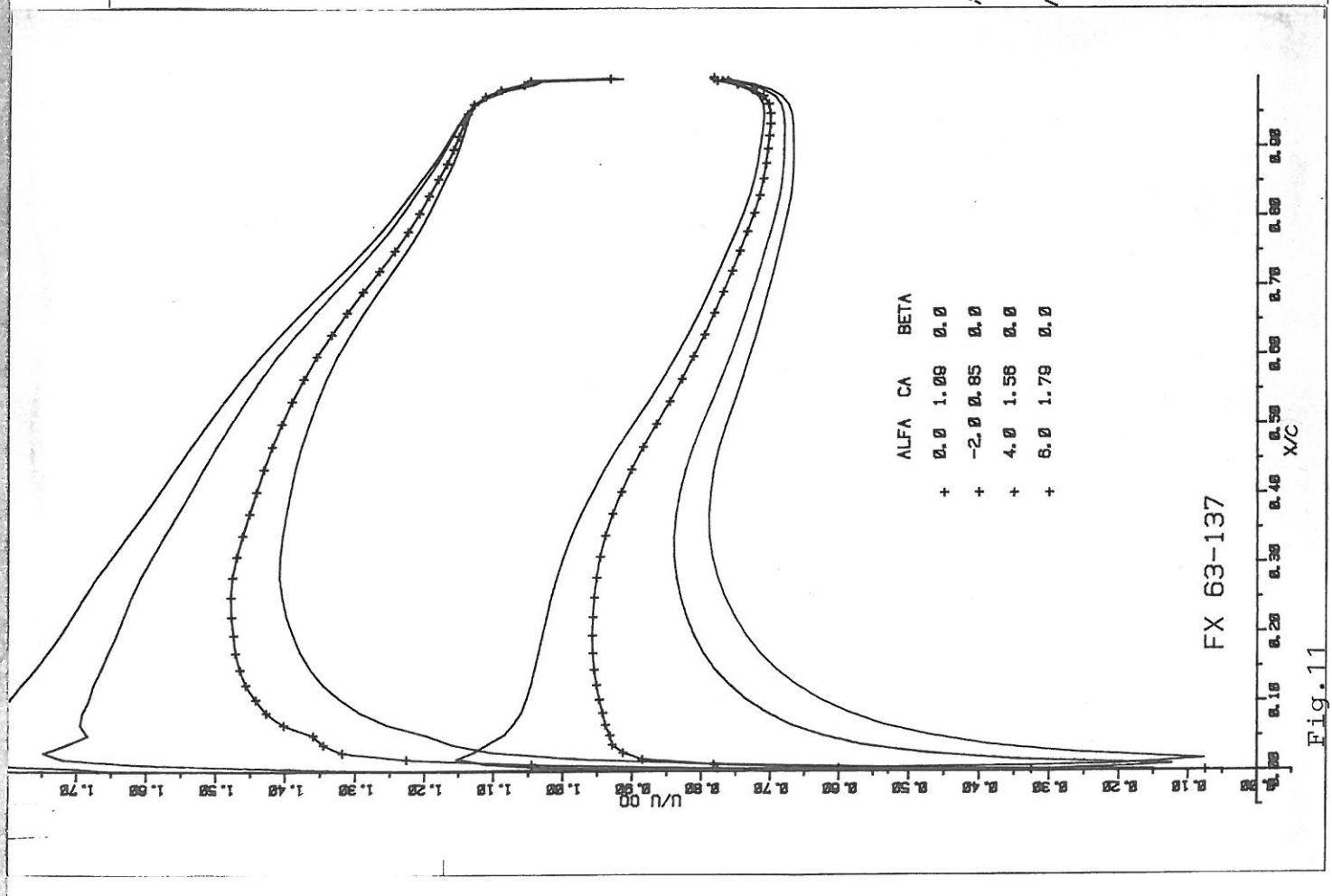
ALFA CA BETA
+ 0.0 1.09 0.0
+ -2.0 0.85 0.0
+ 4.0 1.58 0.0
+ 8.0 1.79 0.0
FX 63-137
u/u∞
X/C

Fig.11

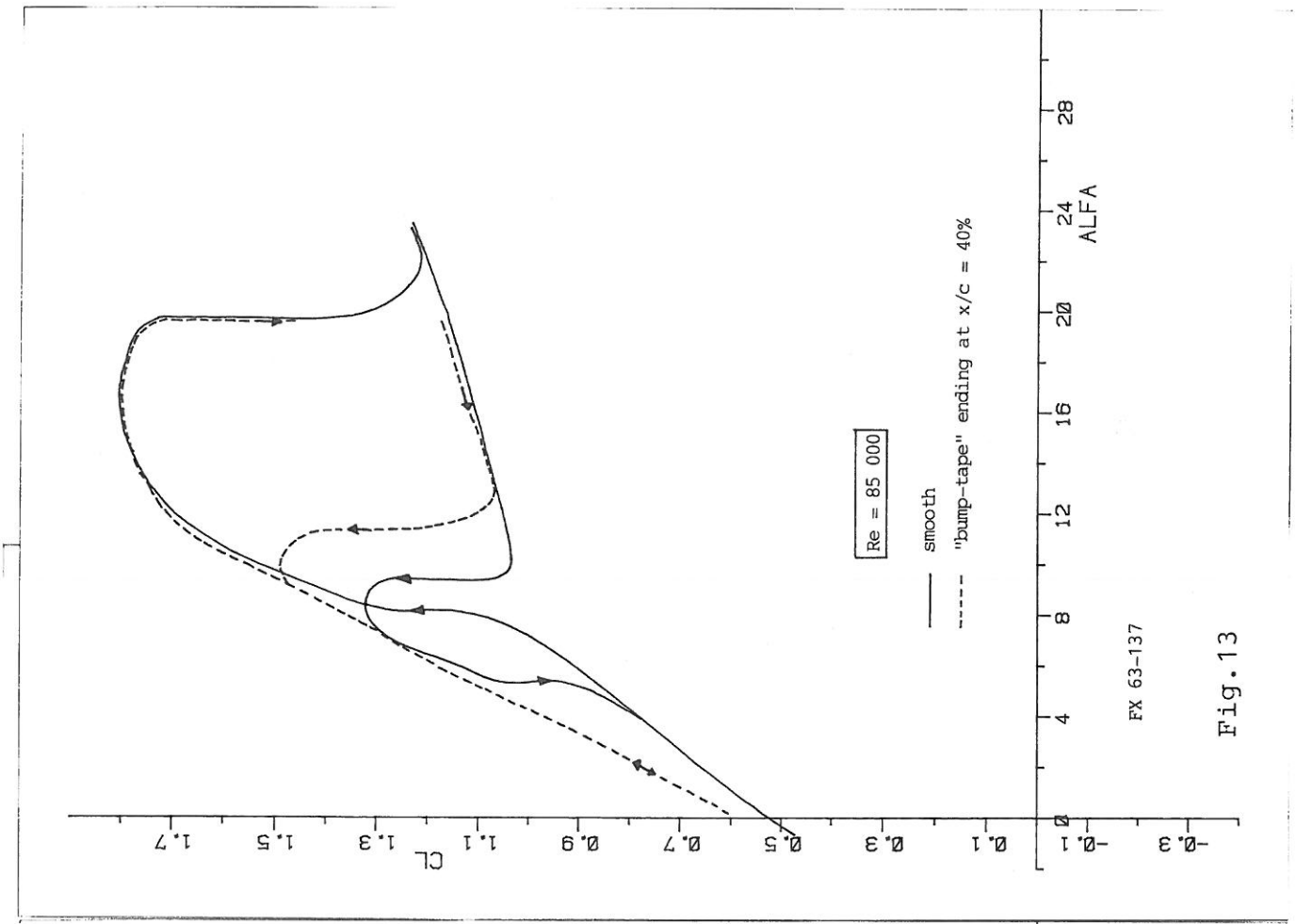
CL
ALFA
Re = 85 000
smooth
"bump-tape" ending at x/c = 40%
FX 63-137

Fig.13

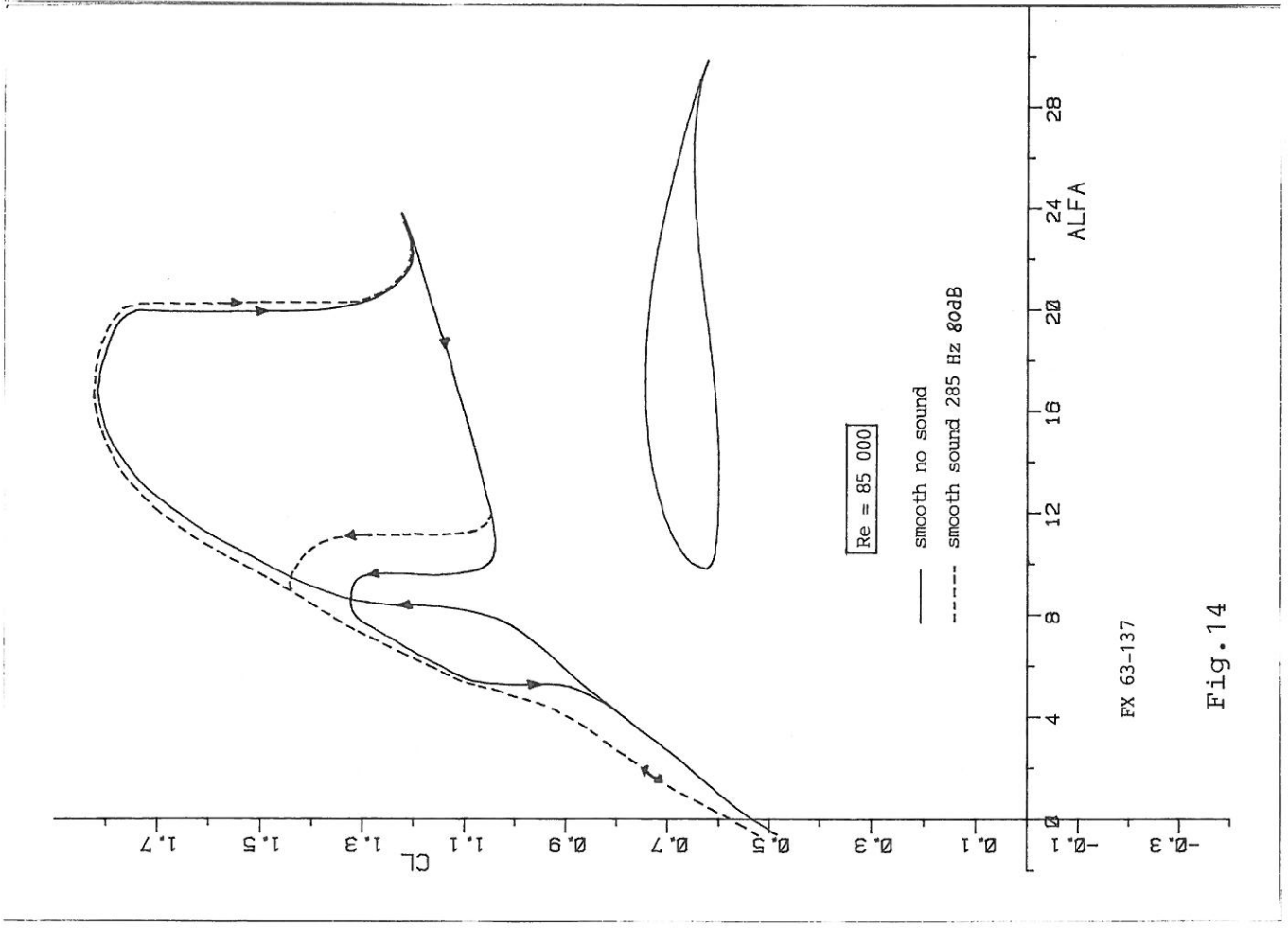
CL
ALFA
Re = 85 000
smooth no sound
smooth sound 285 Hz 80dB
FX 63-137

Fig.14

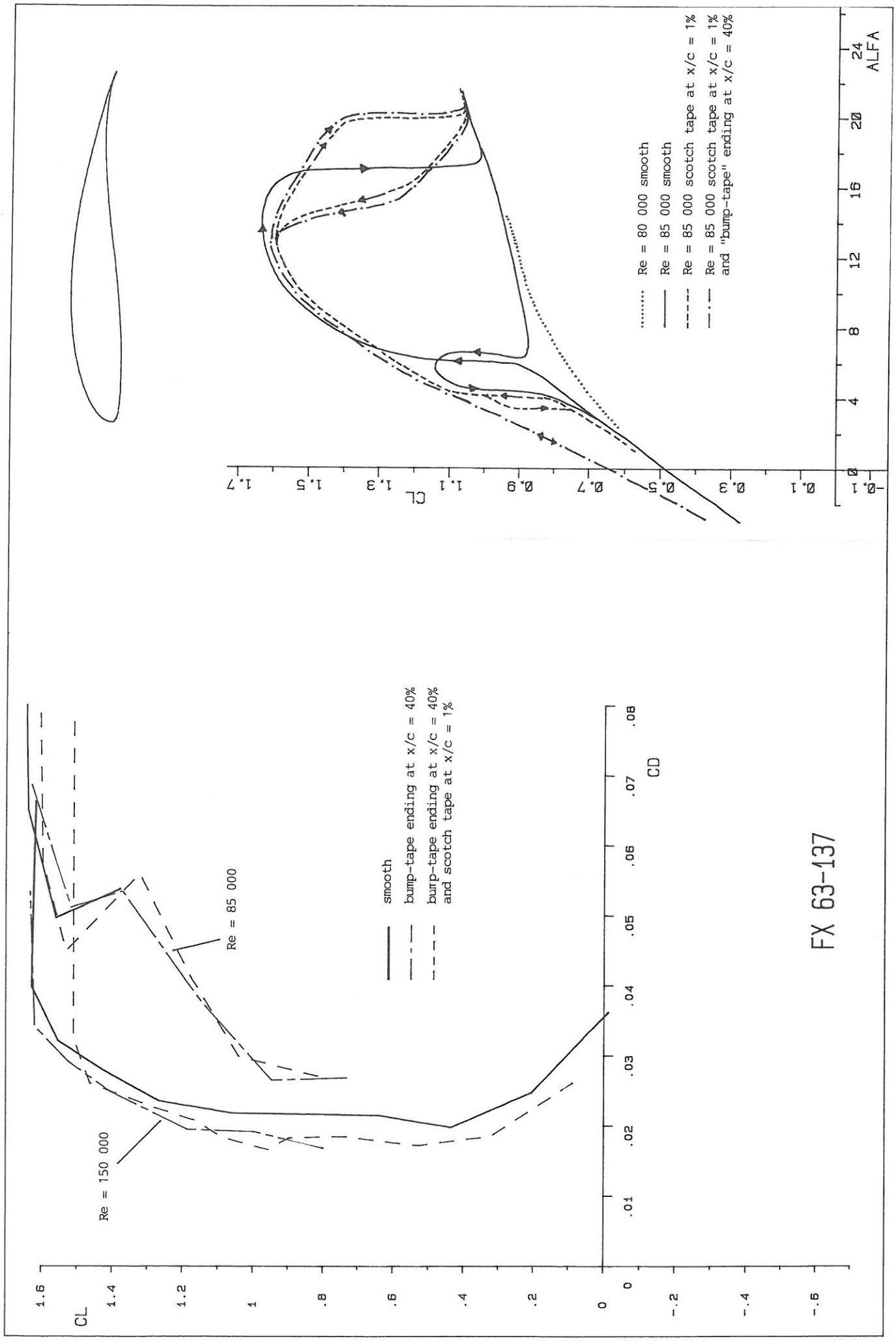
FX 63-137
CL
CD
ALFA
Re = 150 000
Re = 85 000
smooth
bump-tape ending at x/c = 40%
bump-tape ending at x/c = 40%
and scotch tape at x/c = 1%
Re = 80 000 smooth
Re = 85 000 smooth
Re = 85 000 scotch tape at x/c = 1%
Re = 85 000 scotch tape at x/c = 1%
and "bump-tape" ending at x/c = 40%

Fig.16

Fig.15

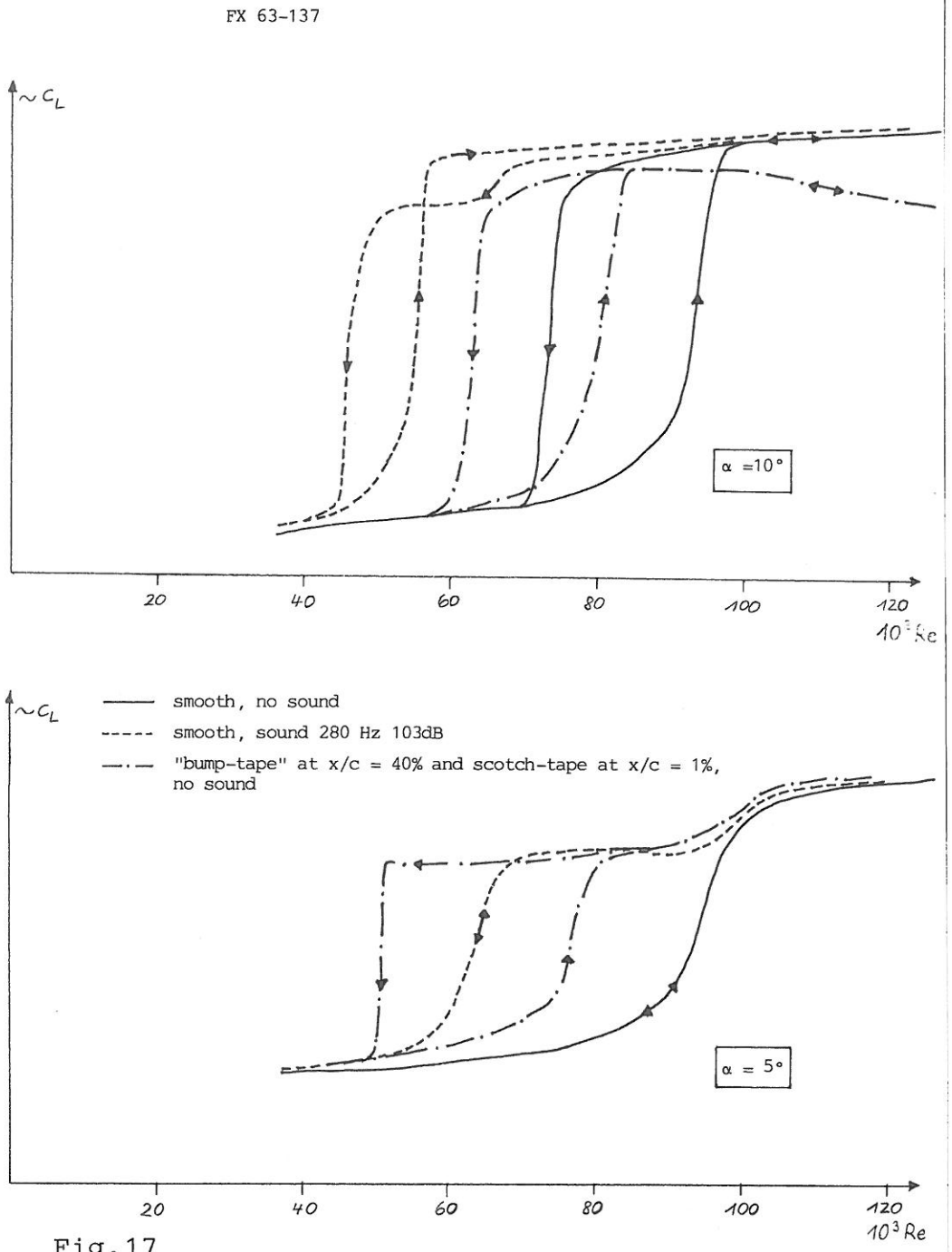

Fig. 17 Lift hysteresis with Reynoldsnumber

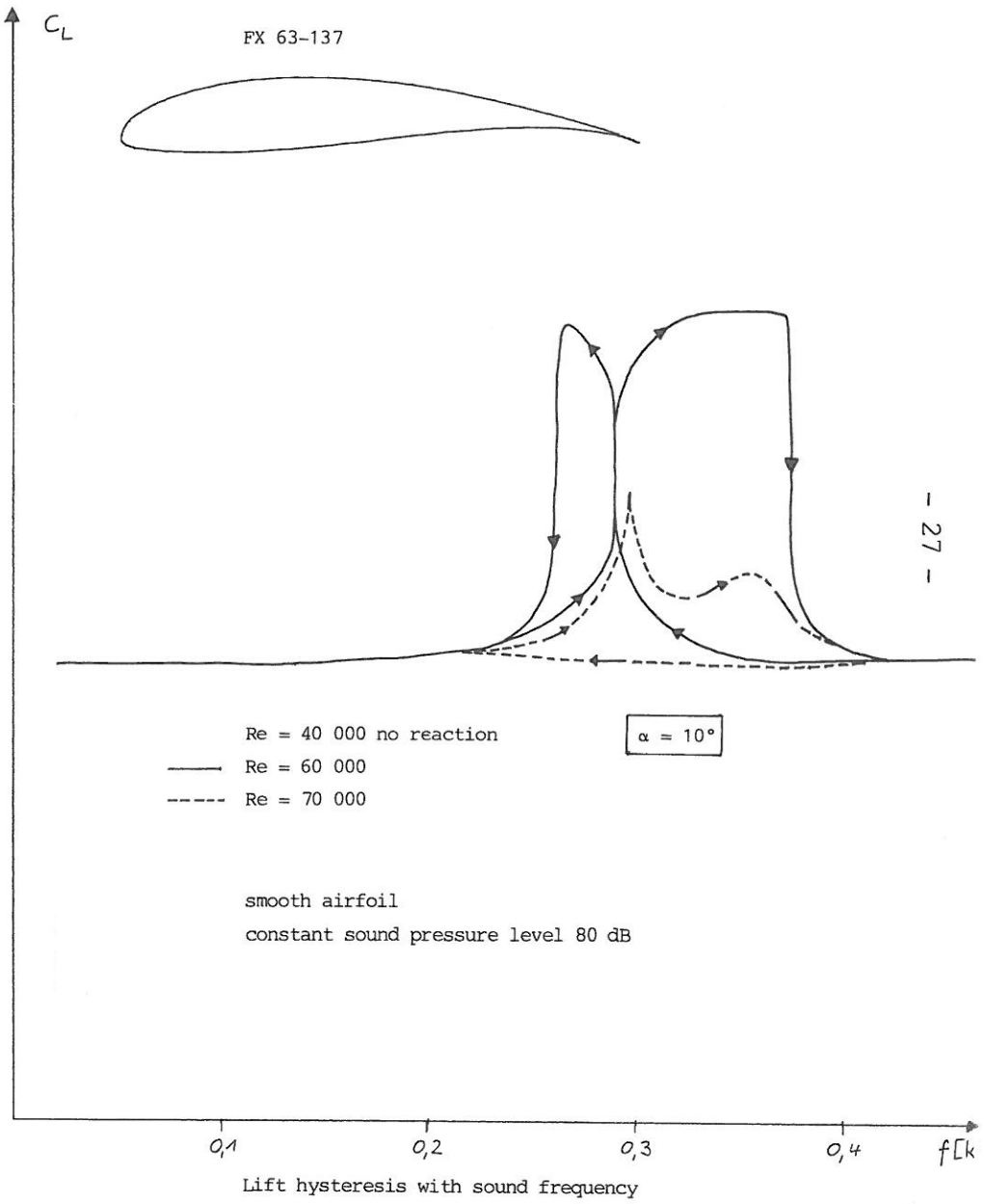

Lift hysteresis with sound frequency

Fig. 18

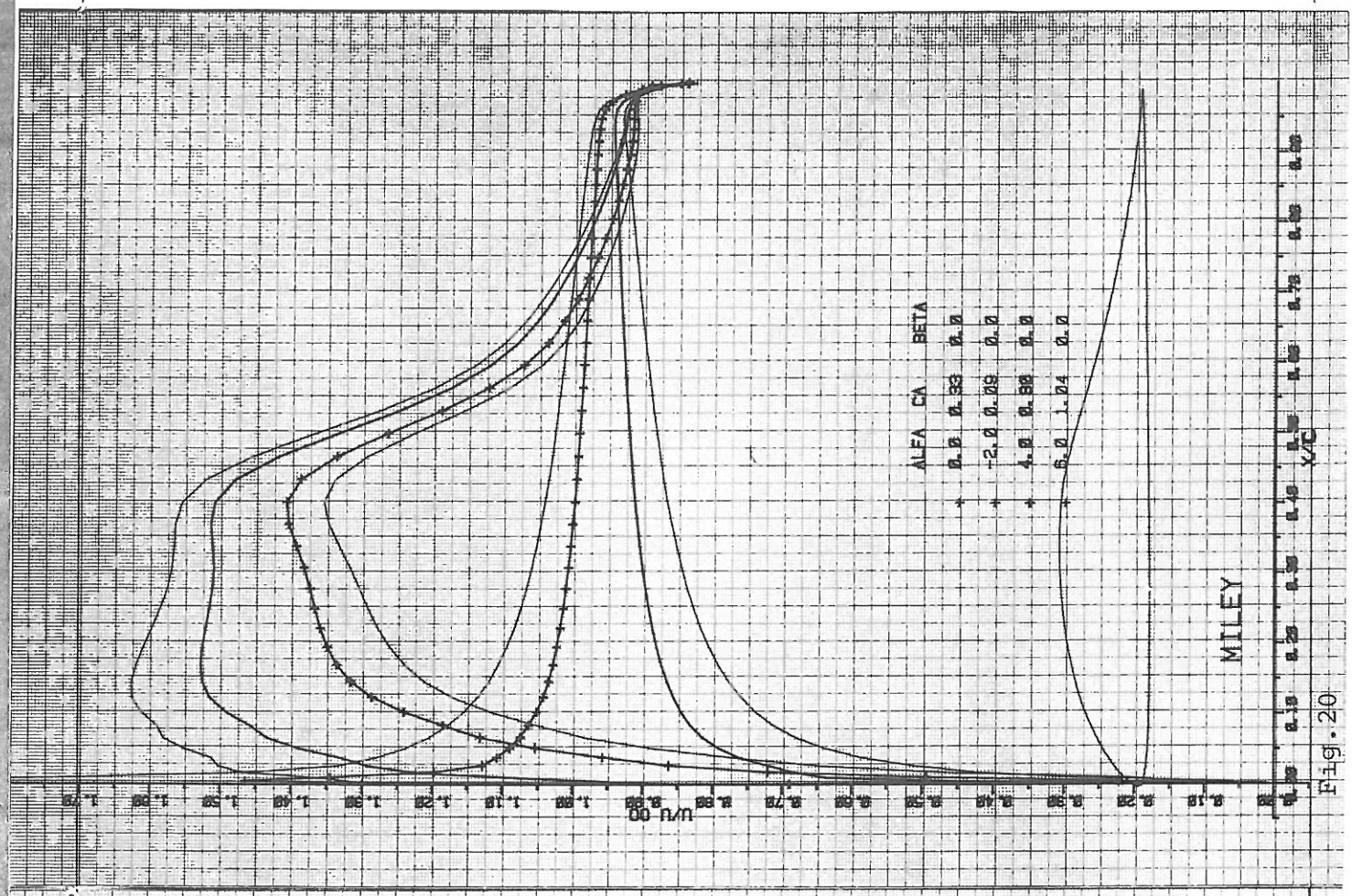
MILEY
ÁLFA CA BETA
0.0 0.33 0.0
+2.0 0.09 0.0
4.0 0.88 0.0
6.0 1.04 0.0
U/U 00
X/C

Fig.20

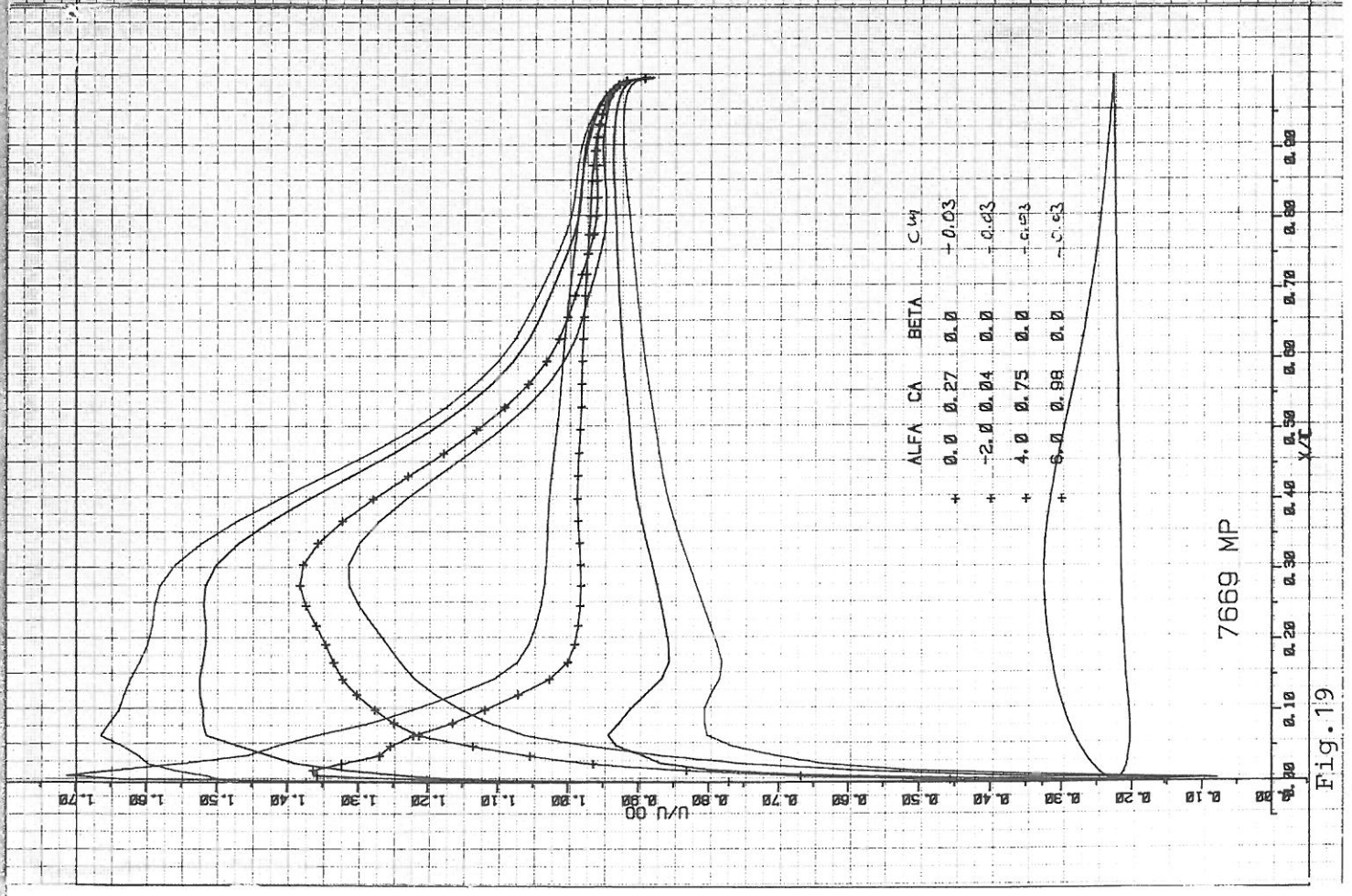
7669 MP
ÁLFA CA BETA Cm
0.0 0.27 0.0 +0.03
-2.0 0.04 0.0 +0.03
4.0 0.75 0.0 -0.03
6.0 0.98 0.0 -0.03
U/U 00
X/C

Fig.19

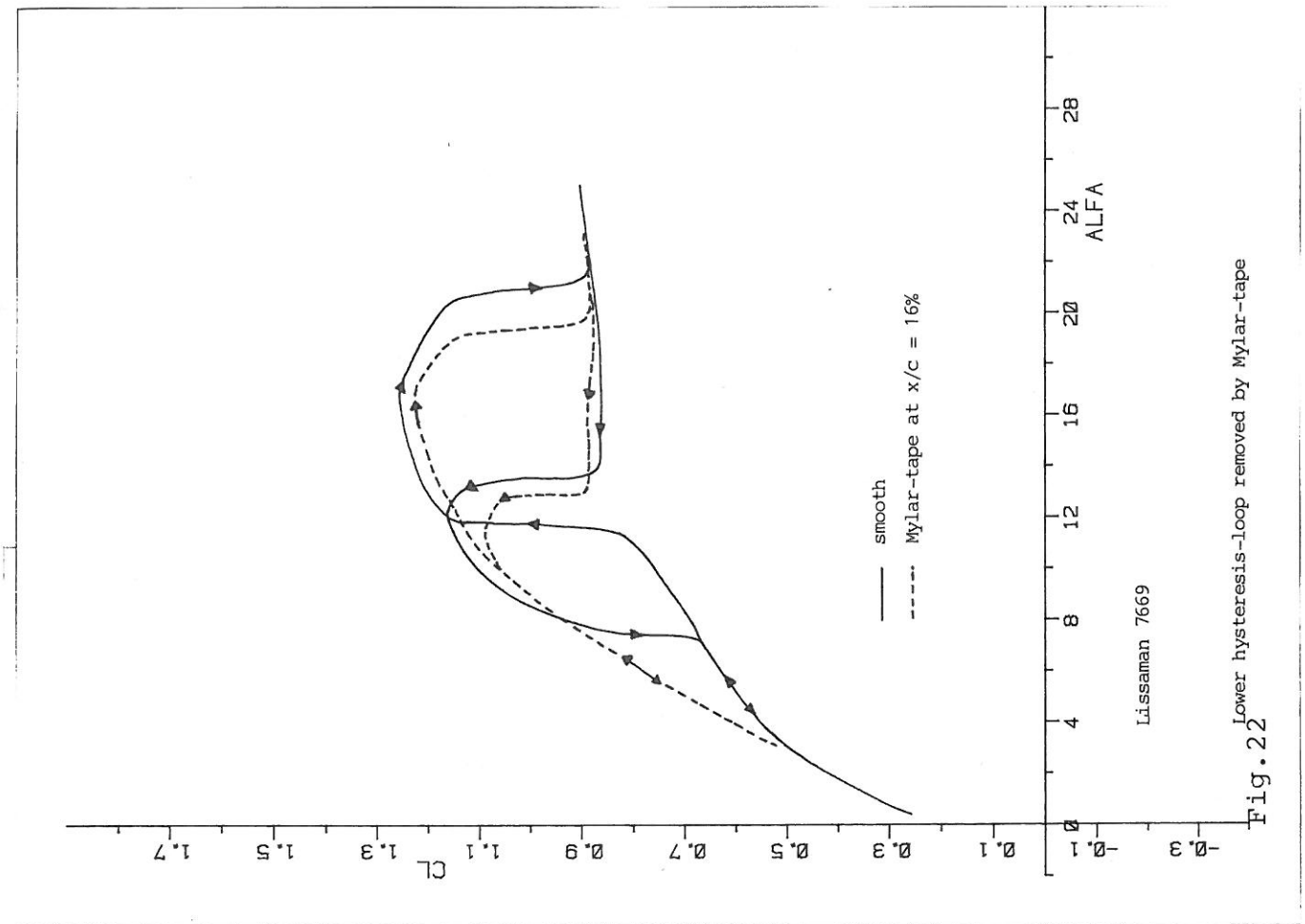

Fig. 22 Lower hysteresis-loop removed by Mylar-tape

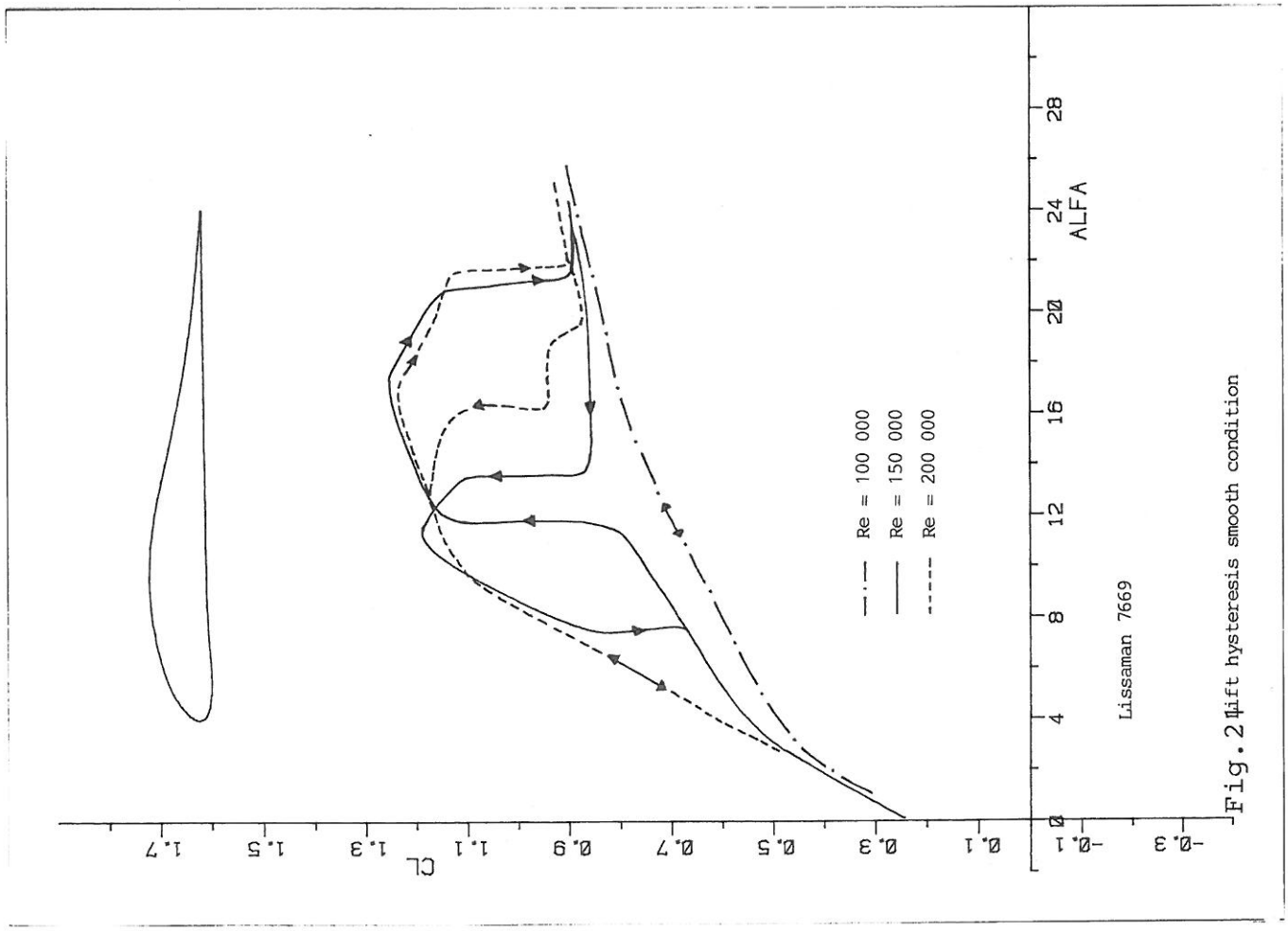

Fig. 23 Lift hysteresis smooth condition

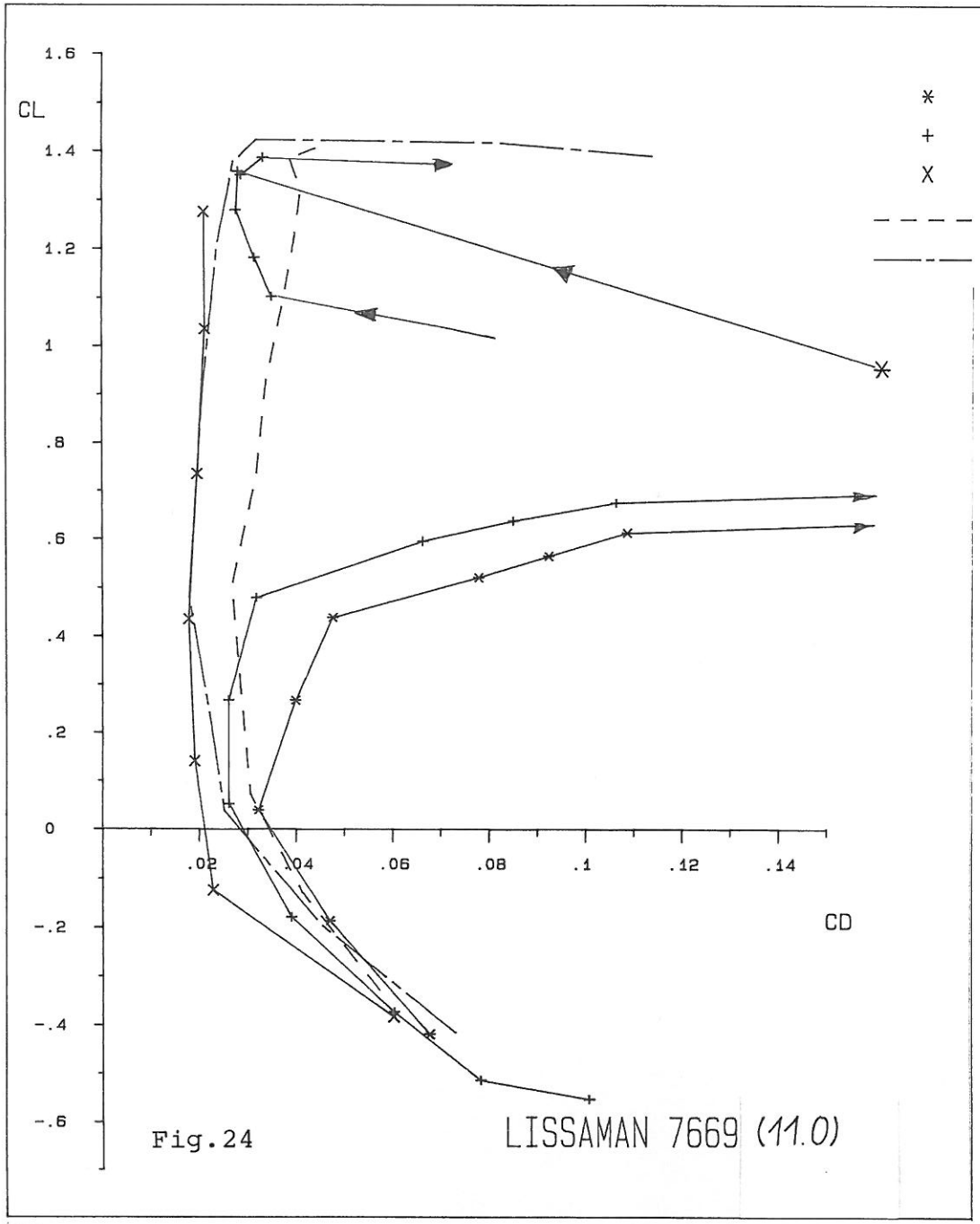

Fig.24 LISSAMAN 7669 (11.0)

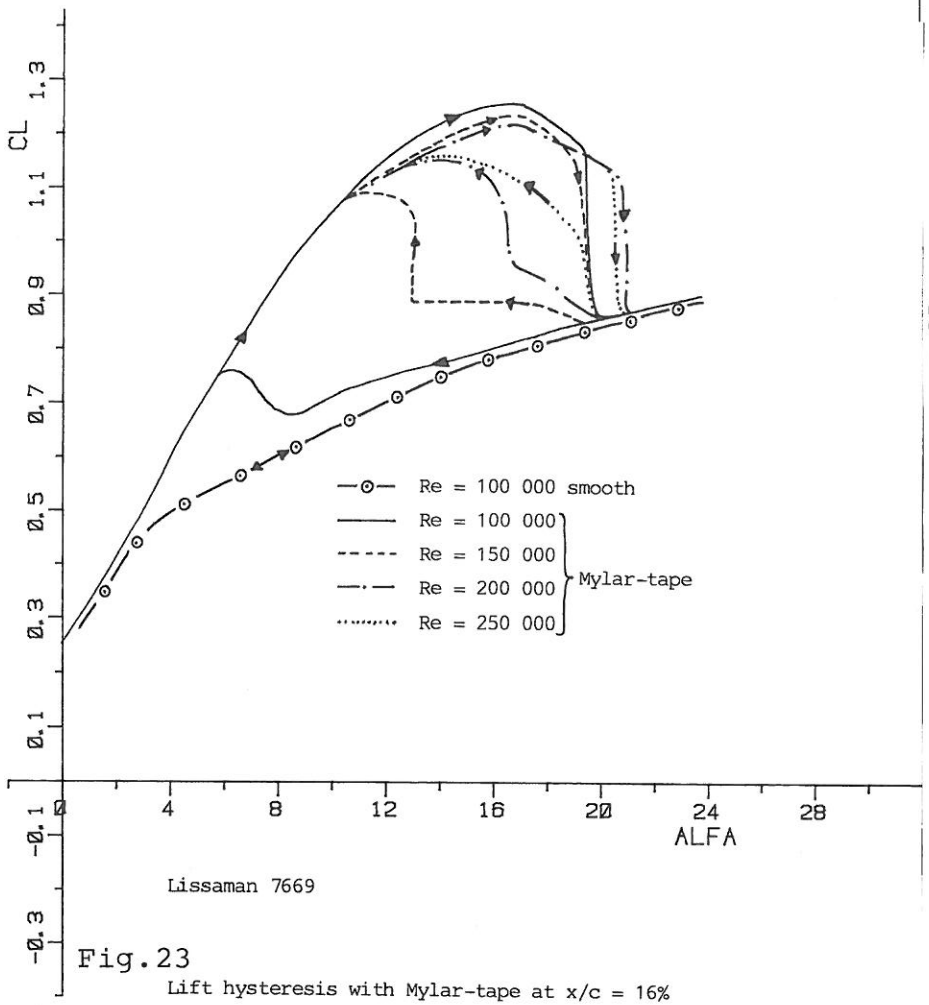

Fig.23
Lift hysteresis with Mylar-tape at x/c = 16%

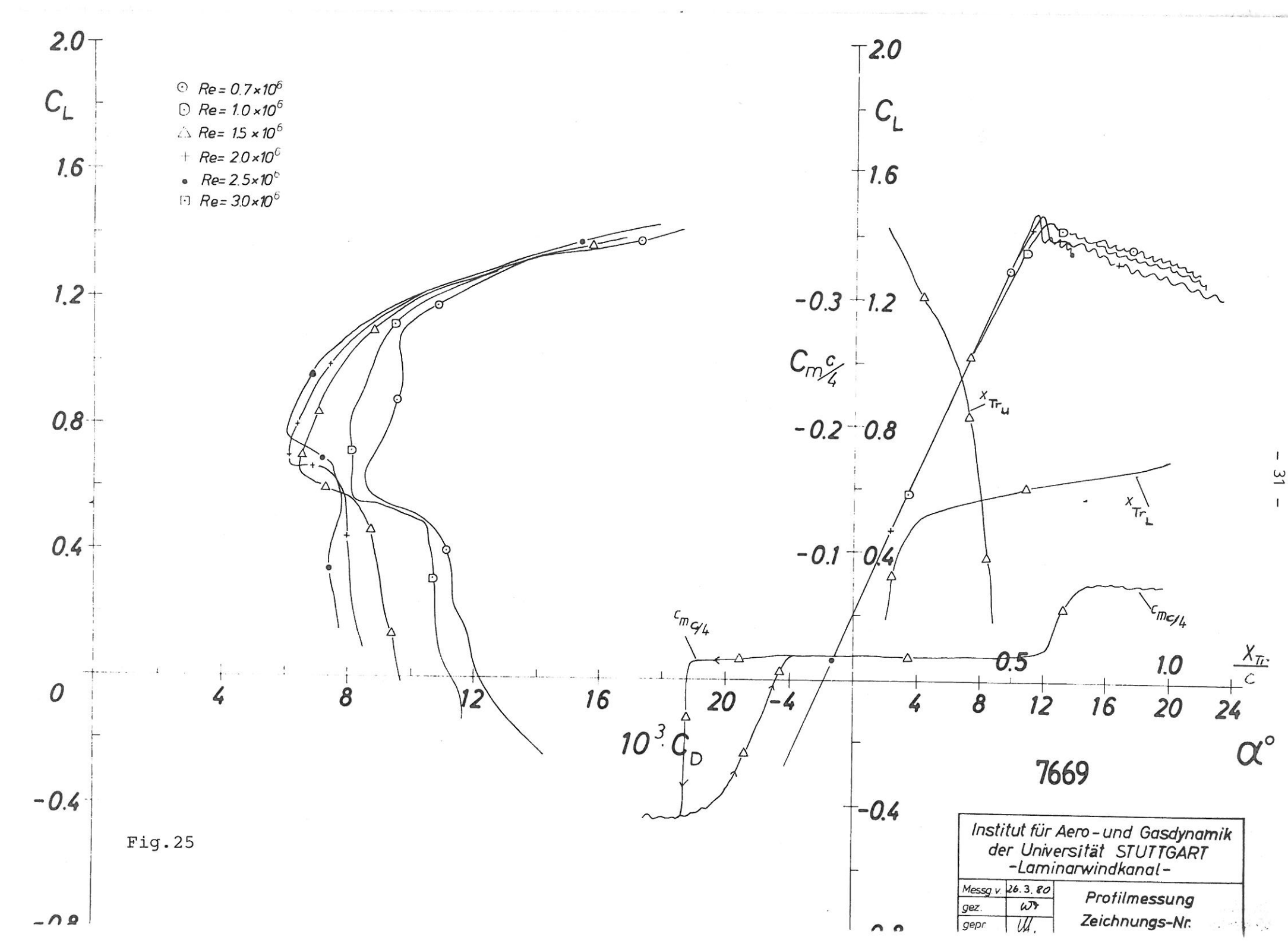

Fig.25

Institut für Aero- und Gasdynamik der Universität STUTTGART -Laminarwindkanal-		
Messg v	26.3.80	Profilmessung
gez.	WS	
gepr		Zeichnungs-Nr.

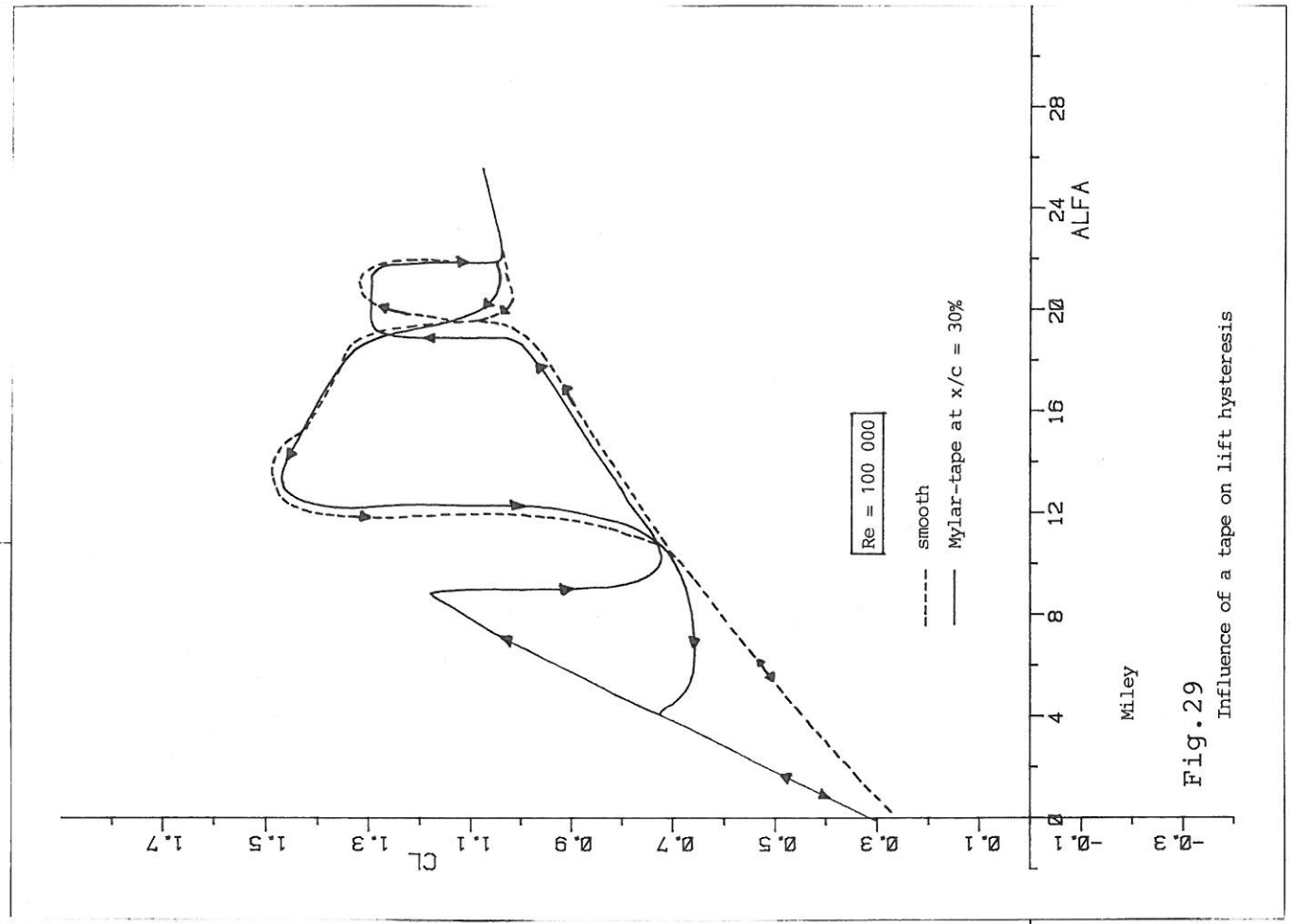

Fig.29 Influence of a tape on lift hysteresis

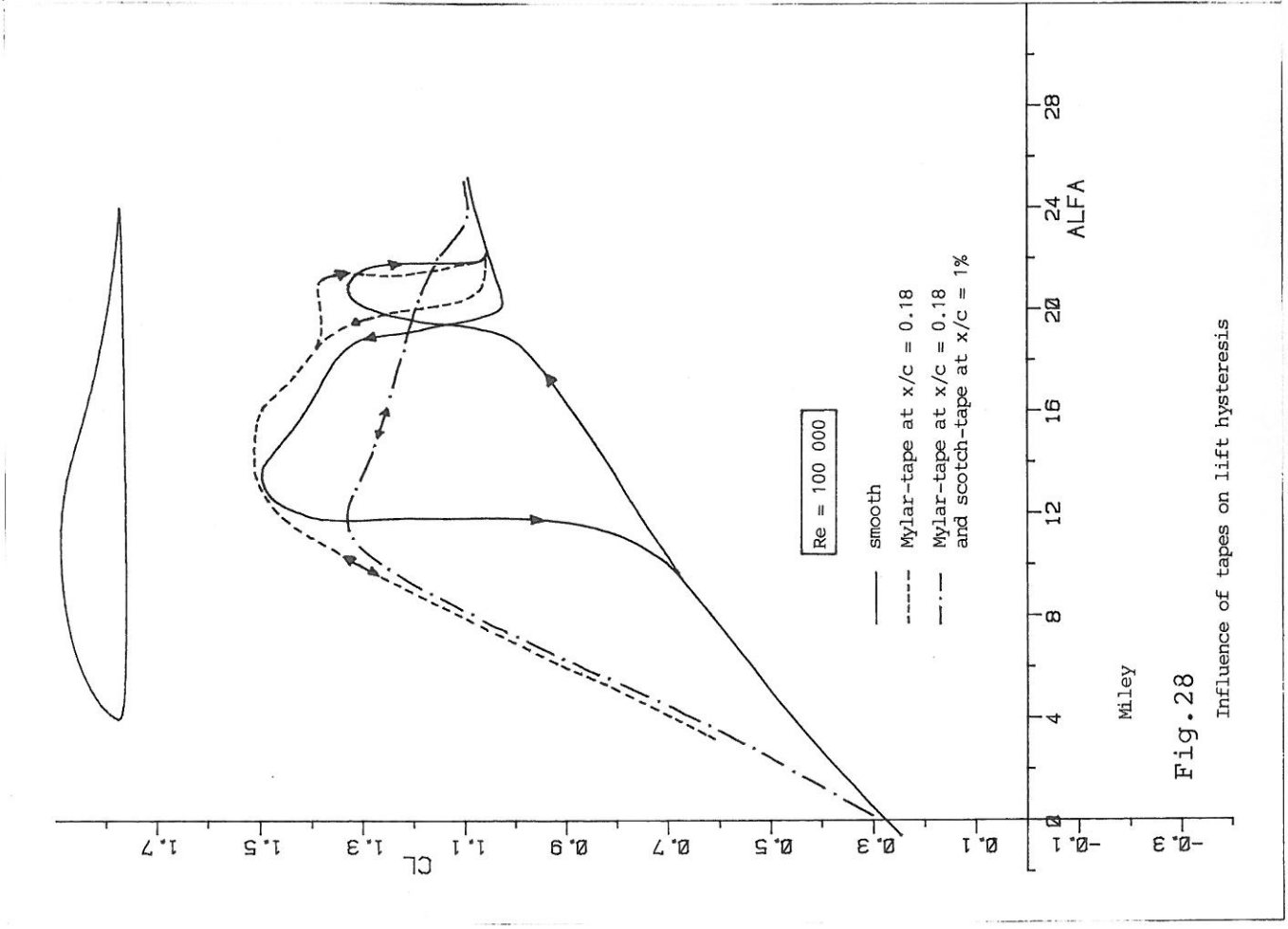

Fig.28 Influence of tapes on lift hysteresis

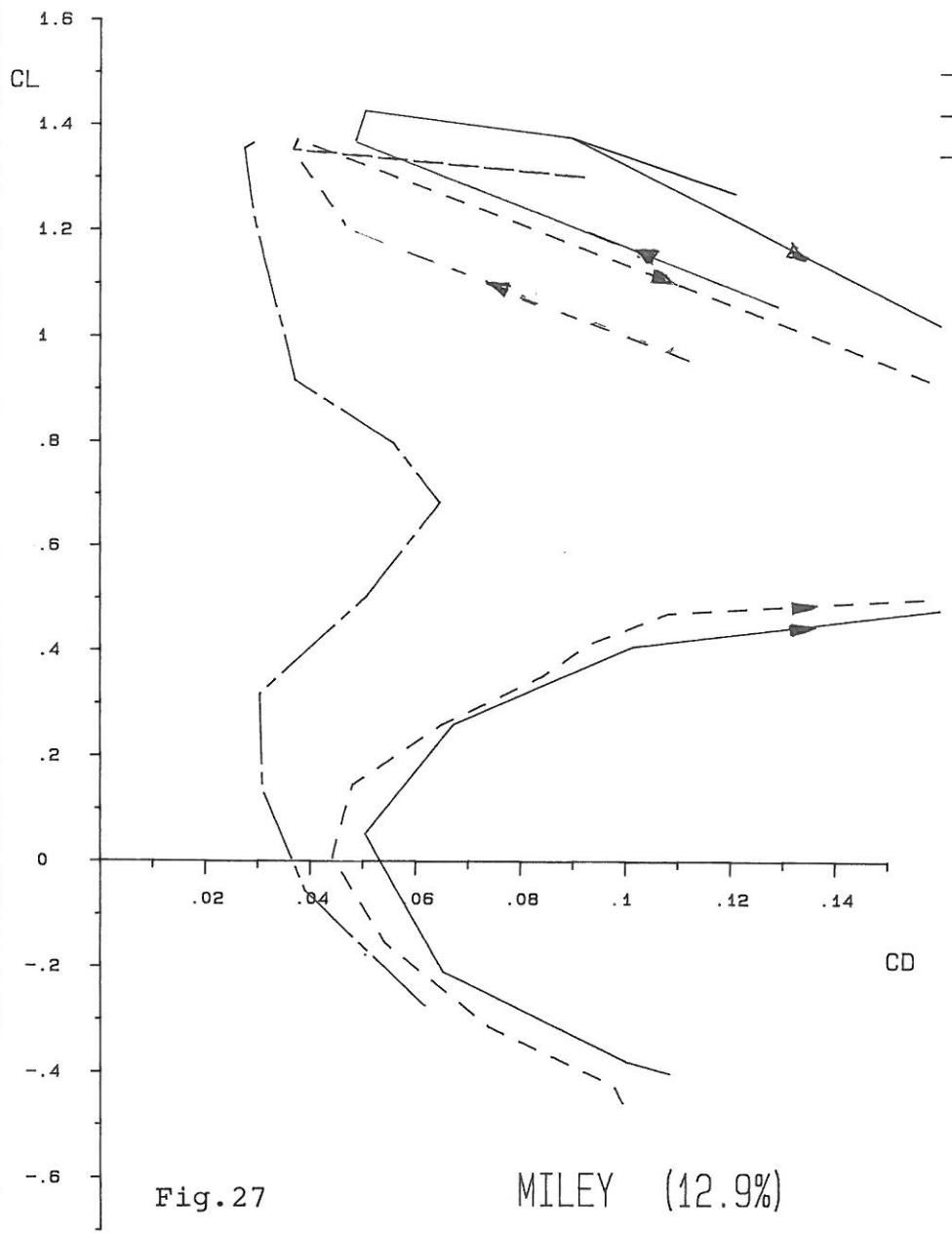

Fig.27 MILEY (12.9%)

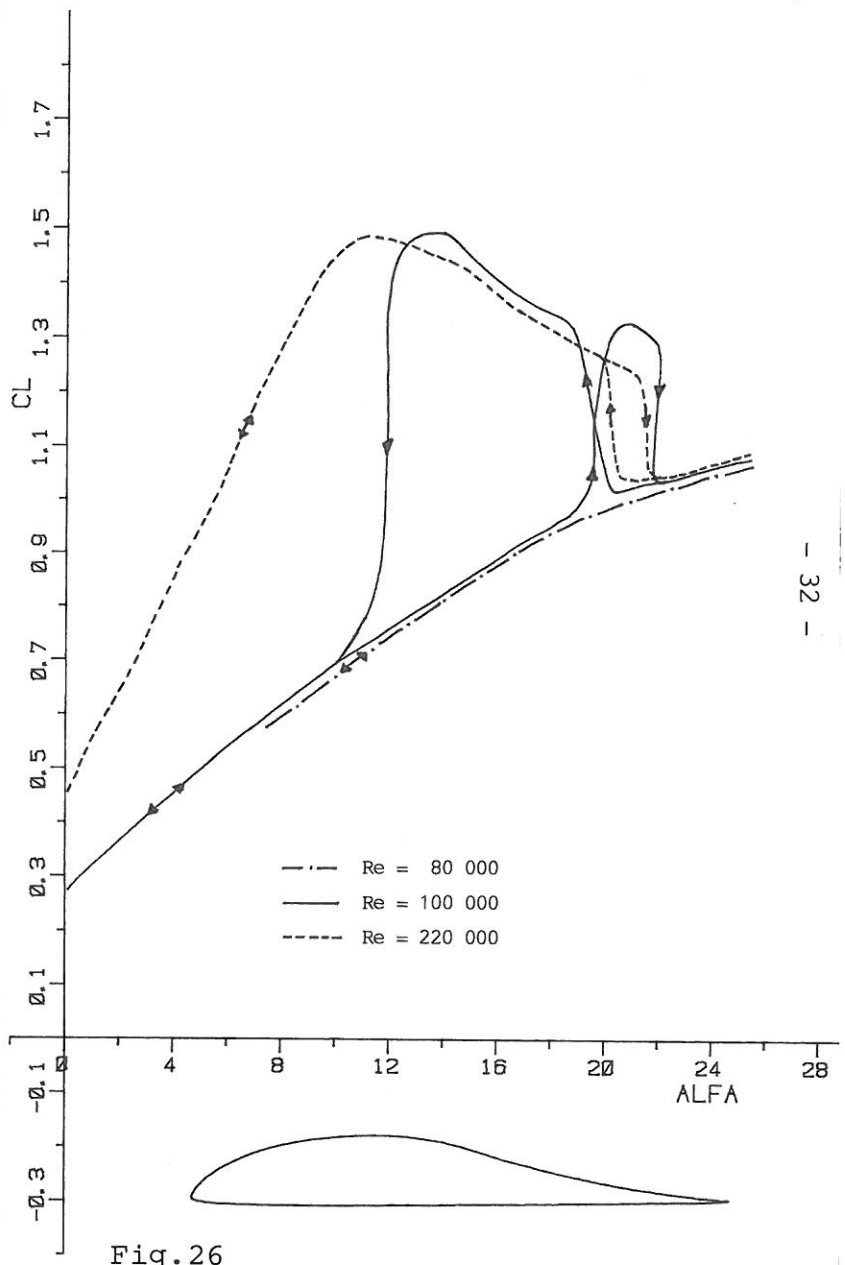

Fig.26

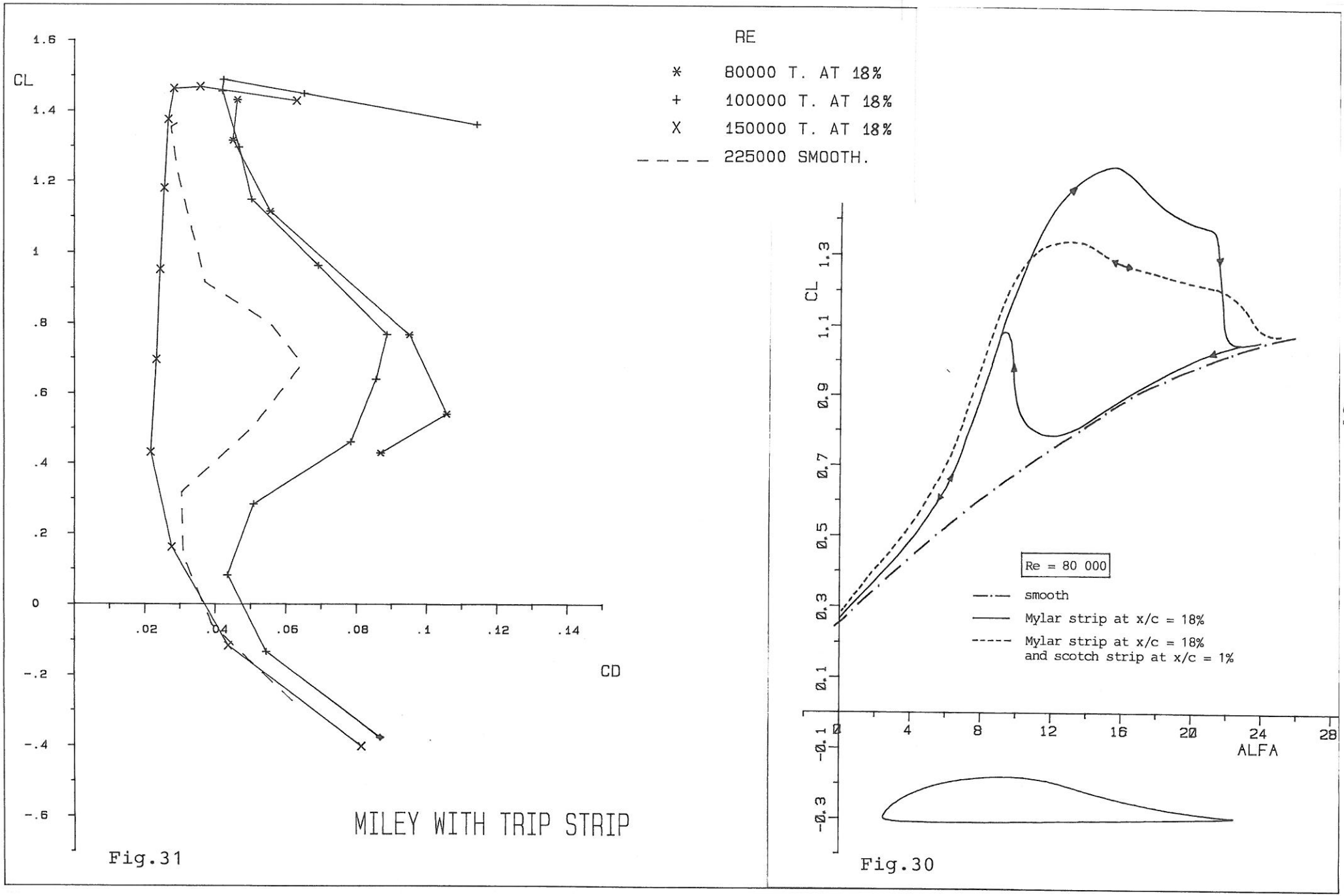
RE
* 80000 T. AT 18%
+ 100000 T. AT 18%
X 150000 T. AT 18%
225000 SMOOTH.
CL
CD
1.6
1.4
1.2
1
.8
.6
.4
.2
0
-.2
-.4
-.6
.02
.04
.06
.08
.1
.12
.14
MILEY WITH TRIP STRIP
Fig.31
CL
ALFA
Re = 80 000
smooth
Mylar strip at x/c = 18%
Mylar strip at x/c = 18%
and scotch strip at x/c = 1%
Fig.30

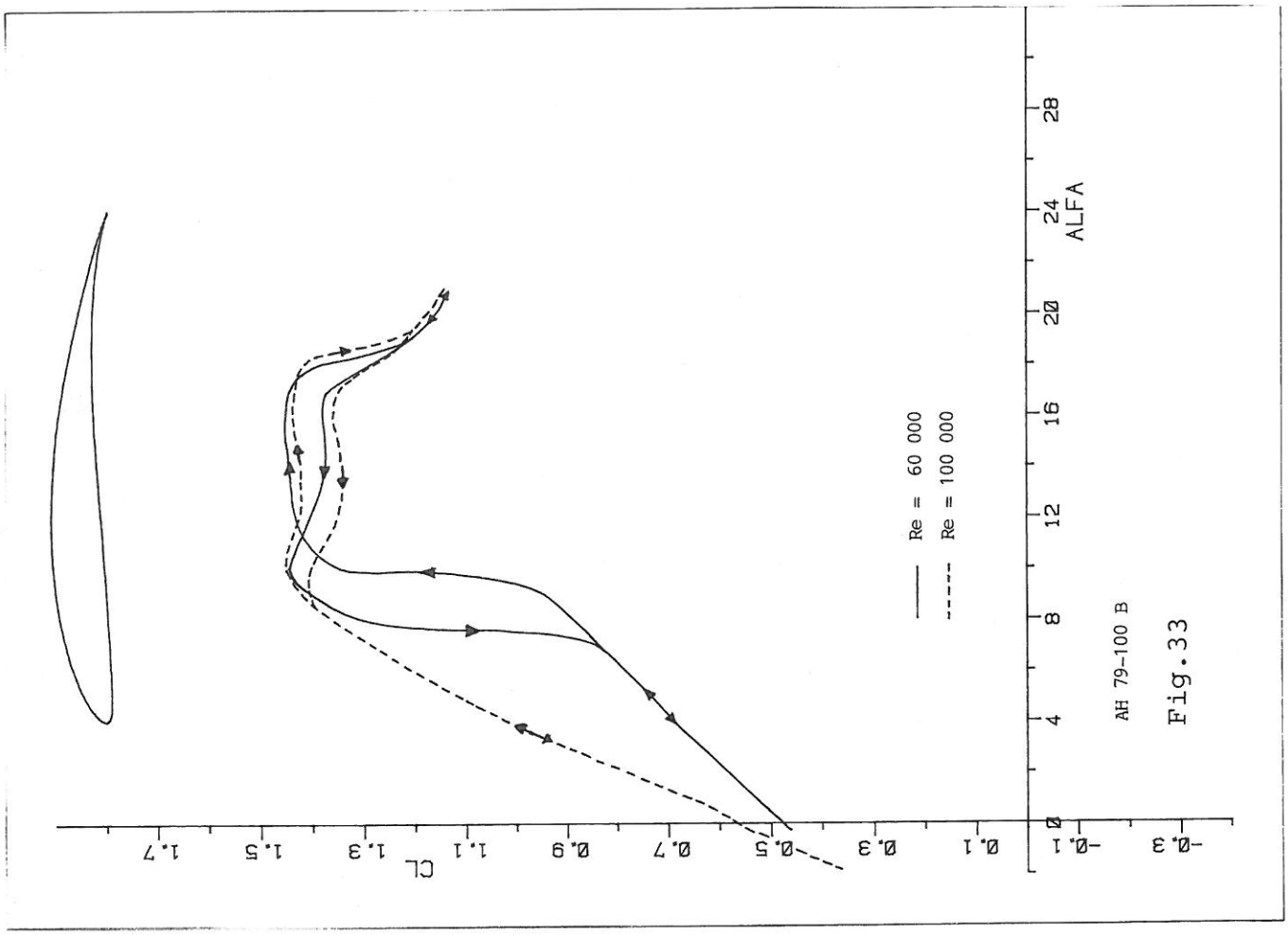

Fig.33

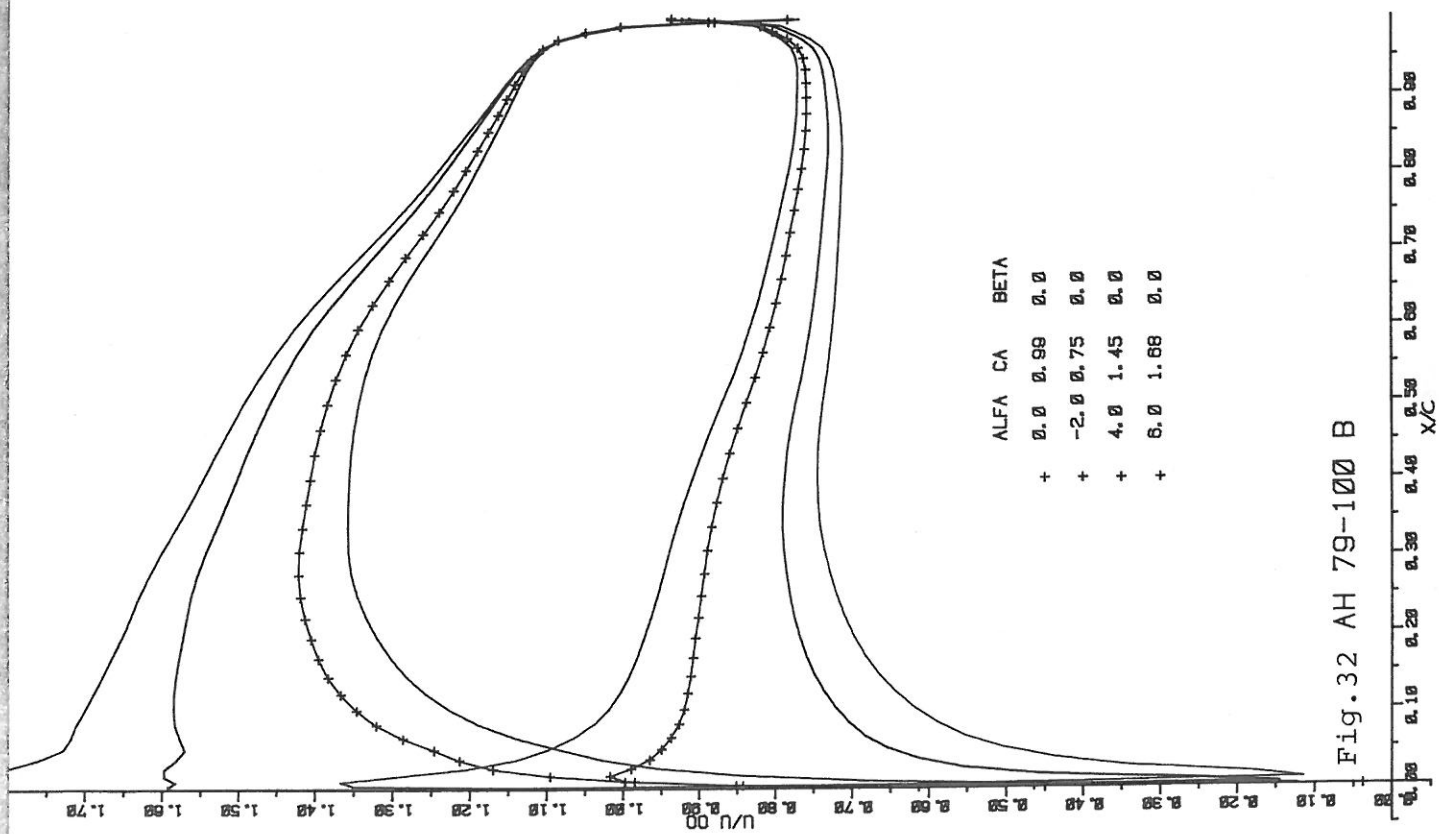

Fig.32 AH 79-100 B

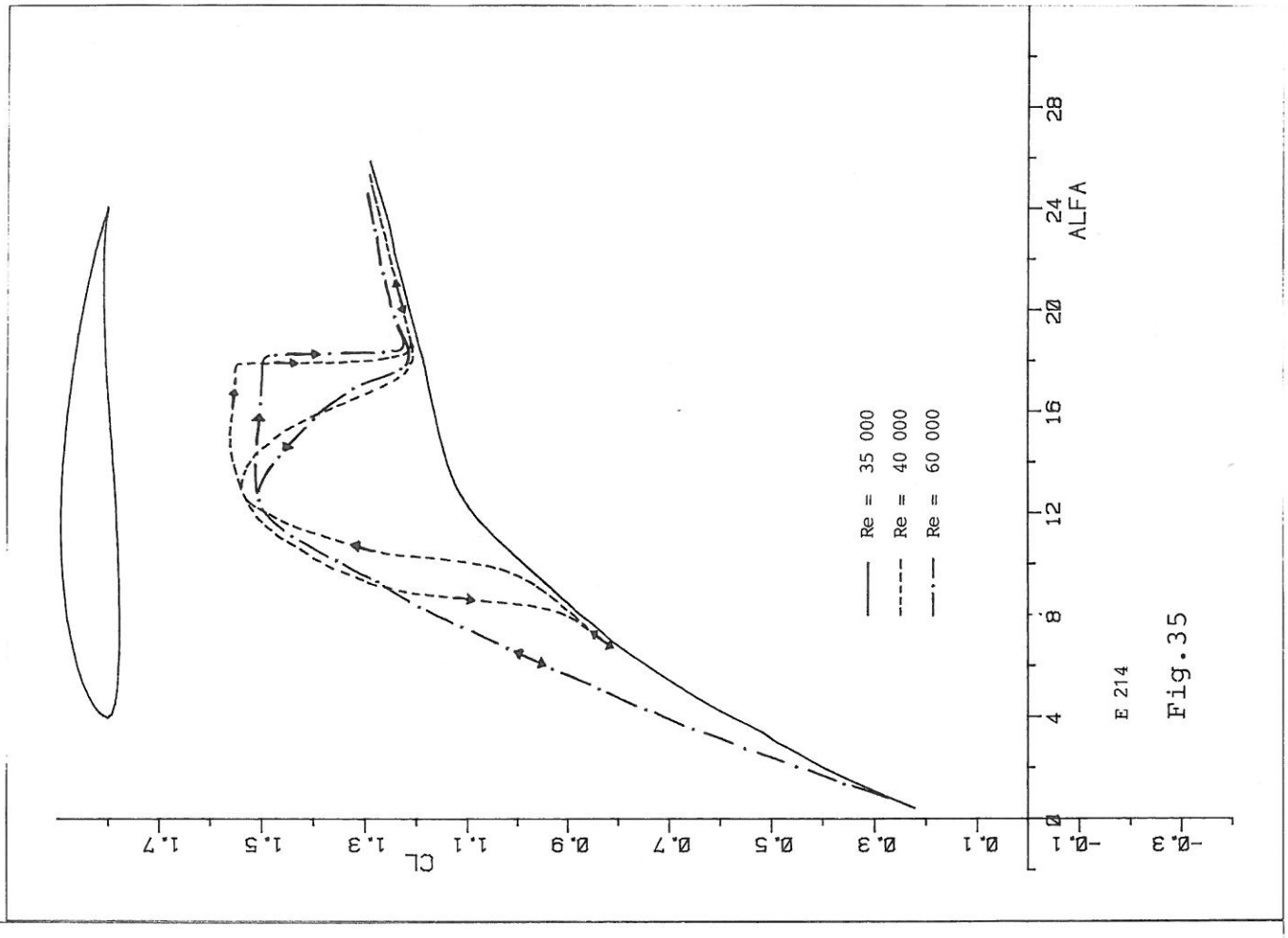

Fig.35

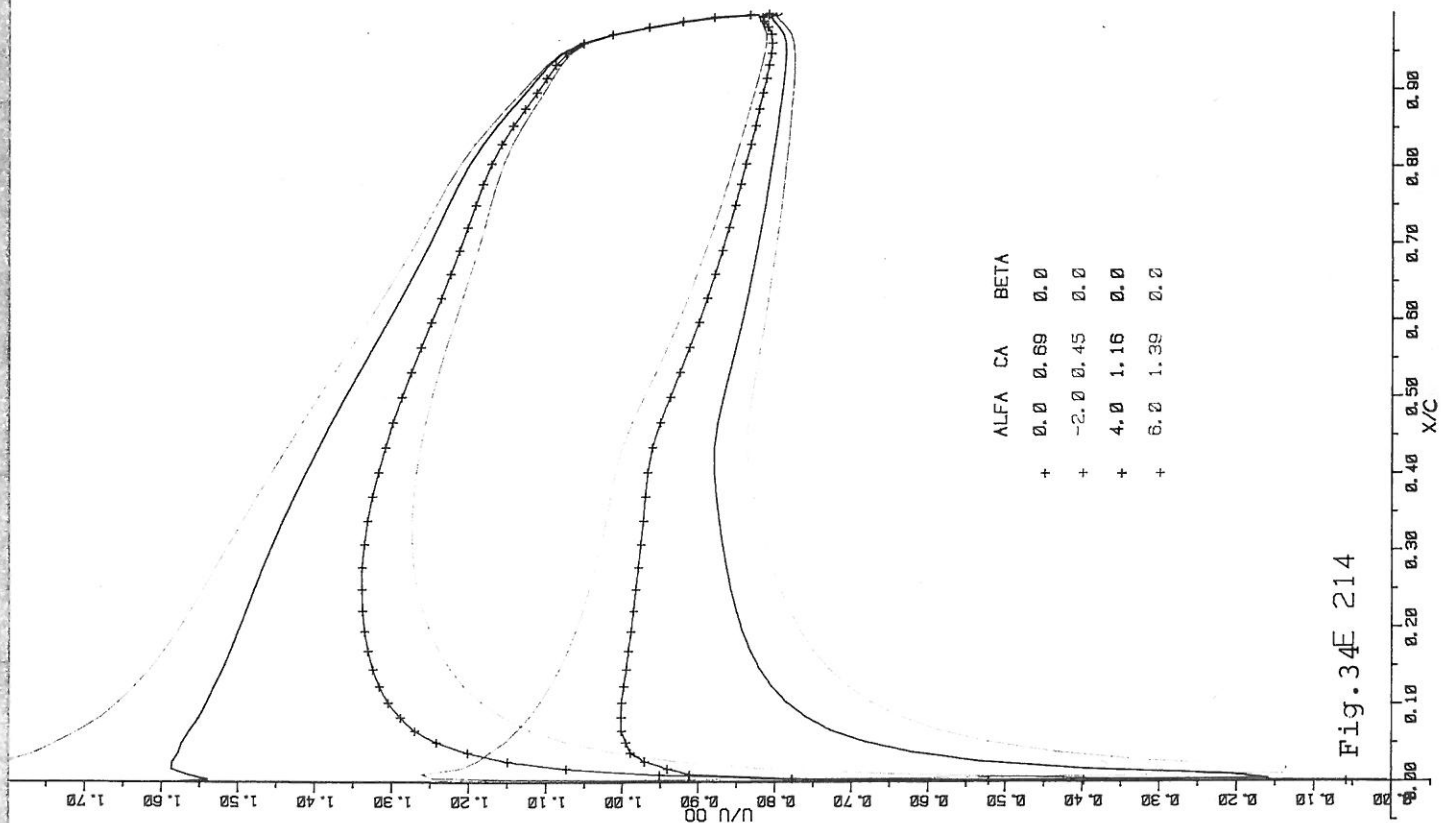

Fig.34E 214

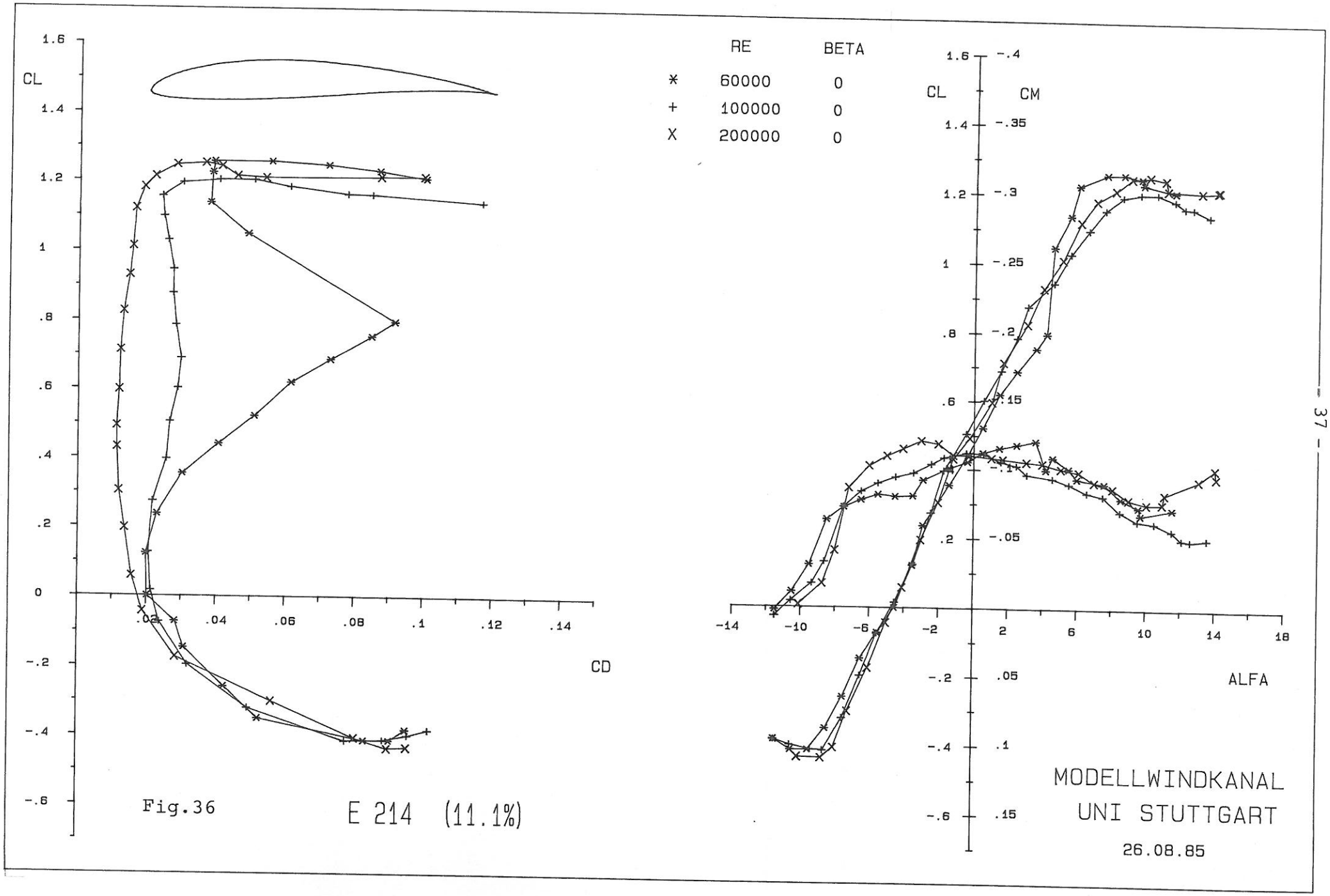

Fig.36 E 214 (11.1%)

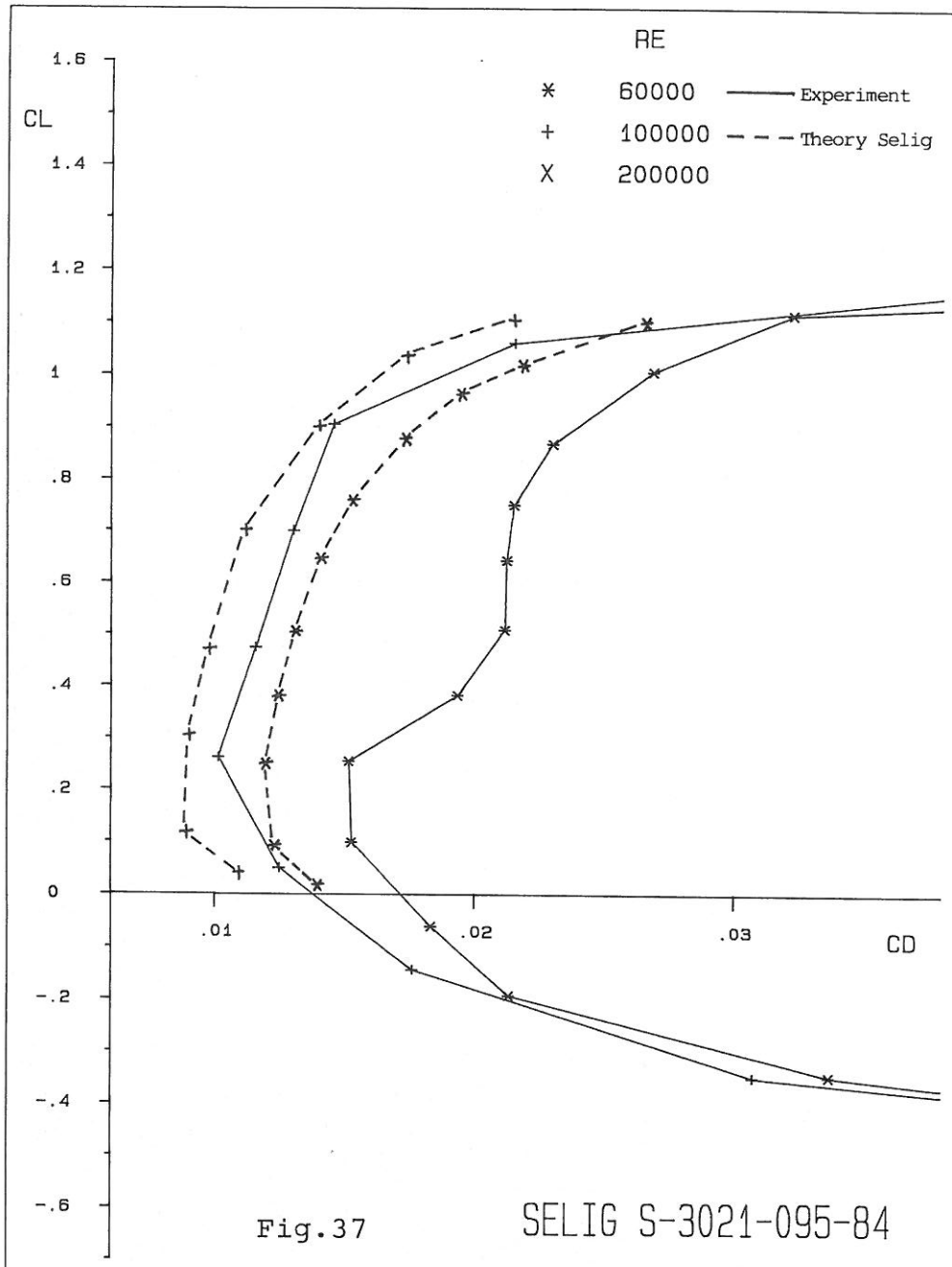

Fig.37 SELIG S-3021-095-84

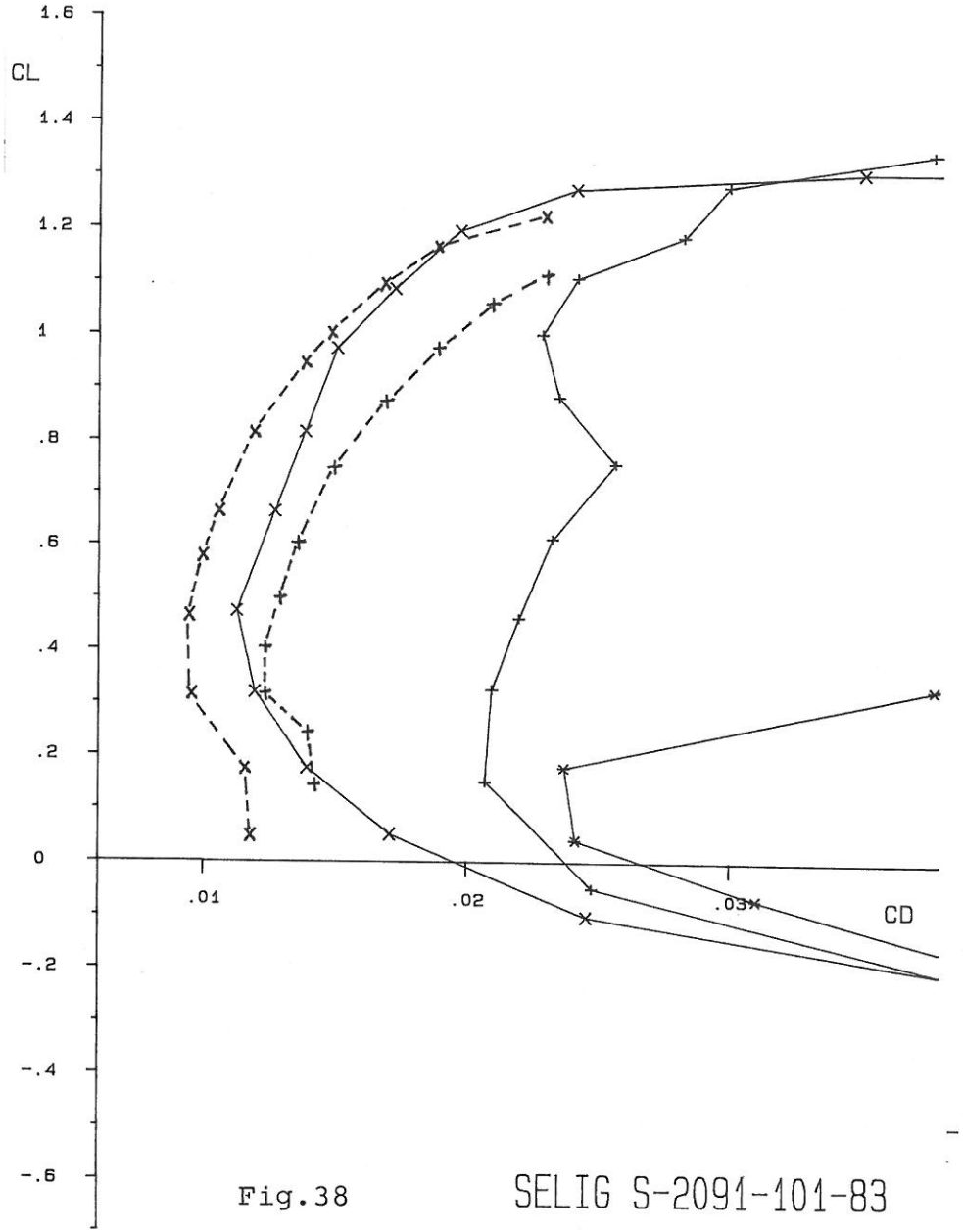

Fig.38 SELIG S-2091-101-83

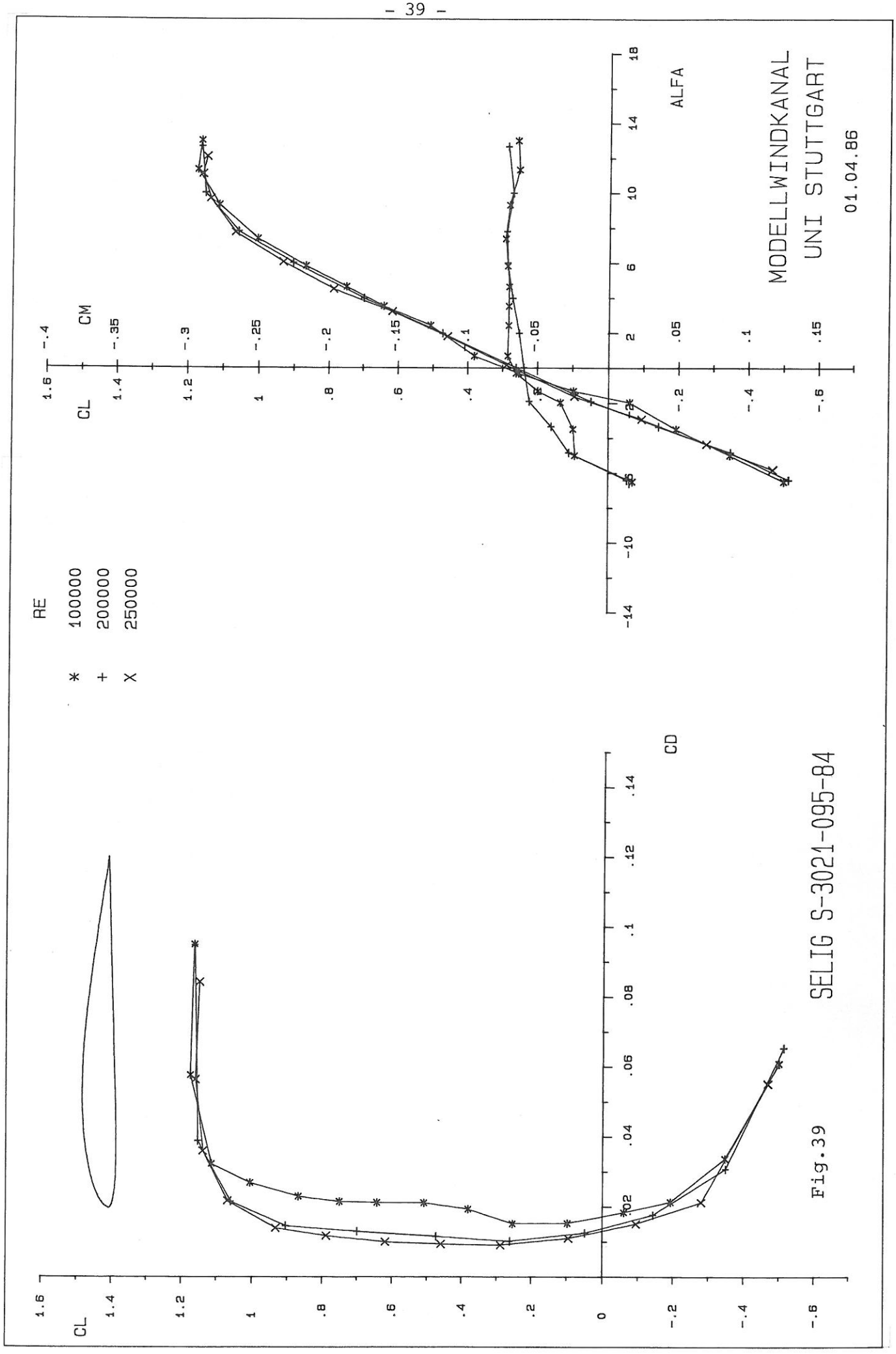
SELIG S-3021-095-84
MODELLWINDKANAL
UNI STUTTGART
01.04.86
RE
* 100000
+ 200000
X 250000
CL
CM
CD
ALFA

Fig.39

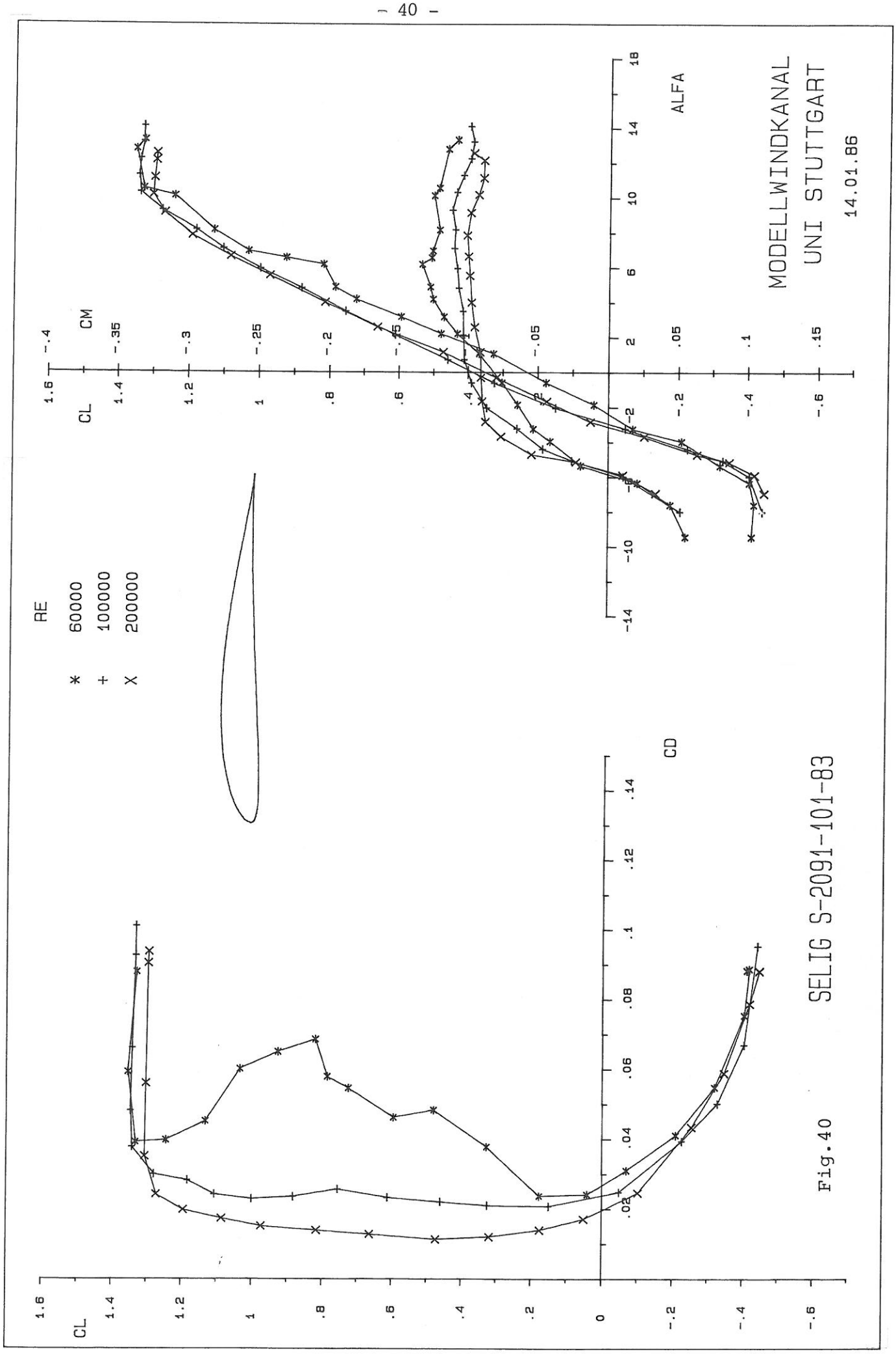
MODELLWINDKANAL
UNI STUTTGART
14.01.86
SELIG S-2091-101-83
RE
* 60000
+ 100000
X 200000
CL
CM
ALFA
CD

Fig.40

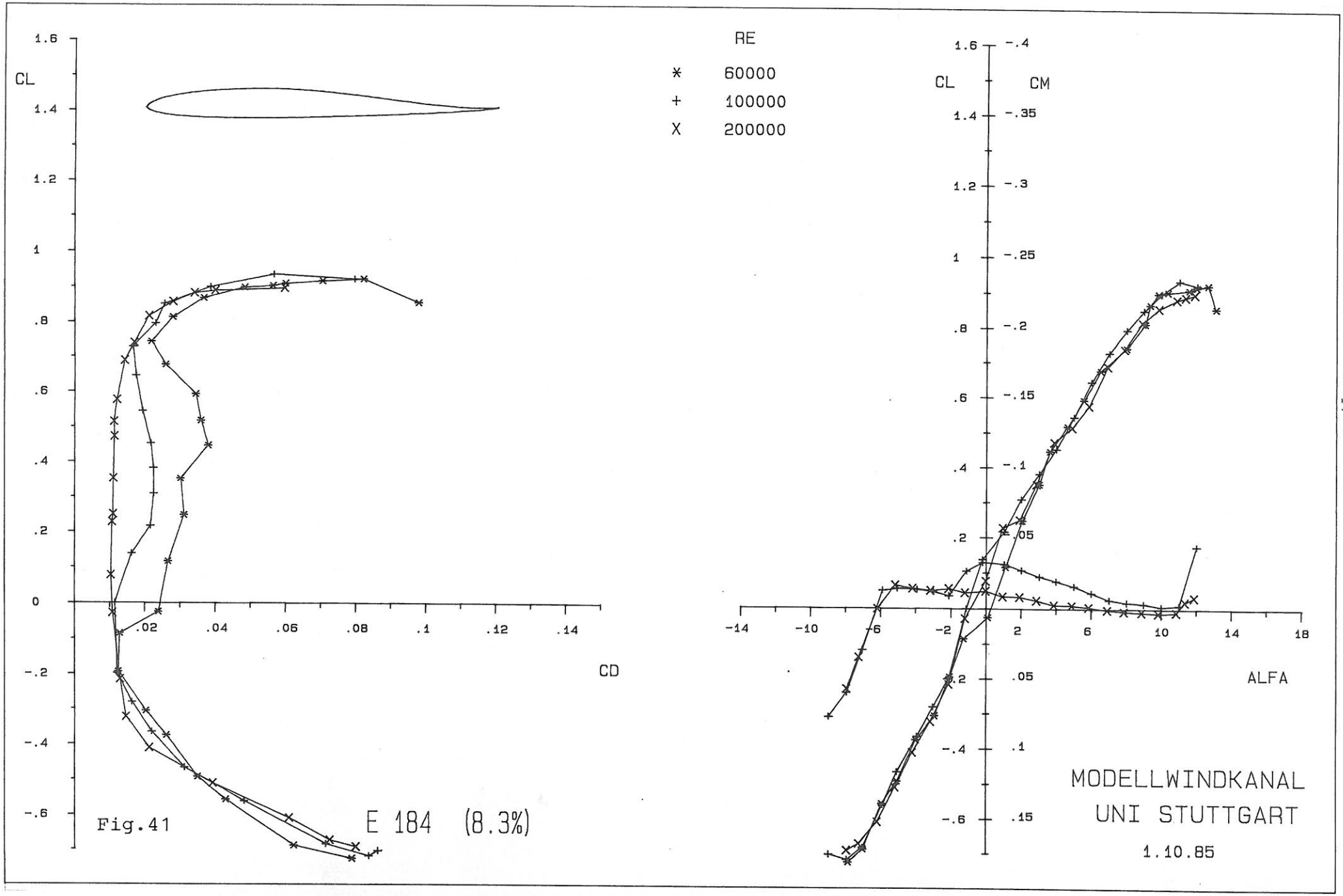

Fig.41 E 184 (8.3%)

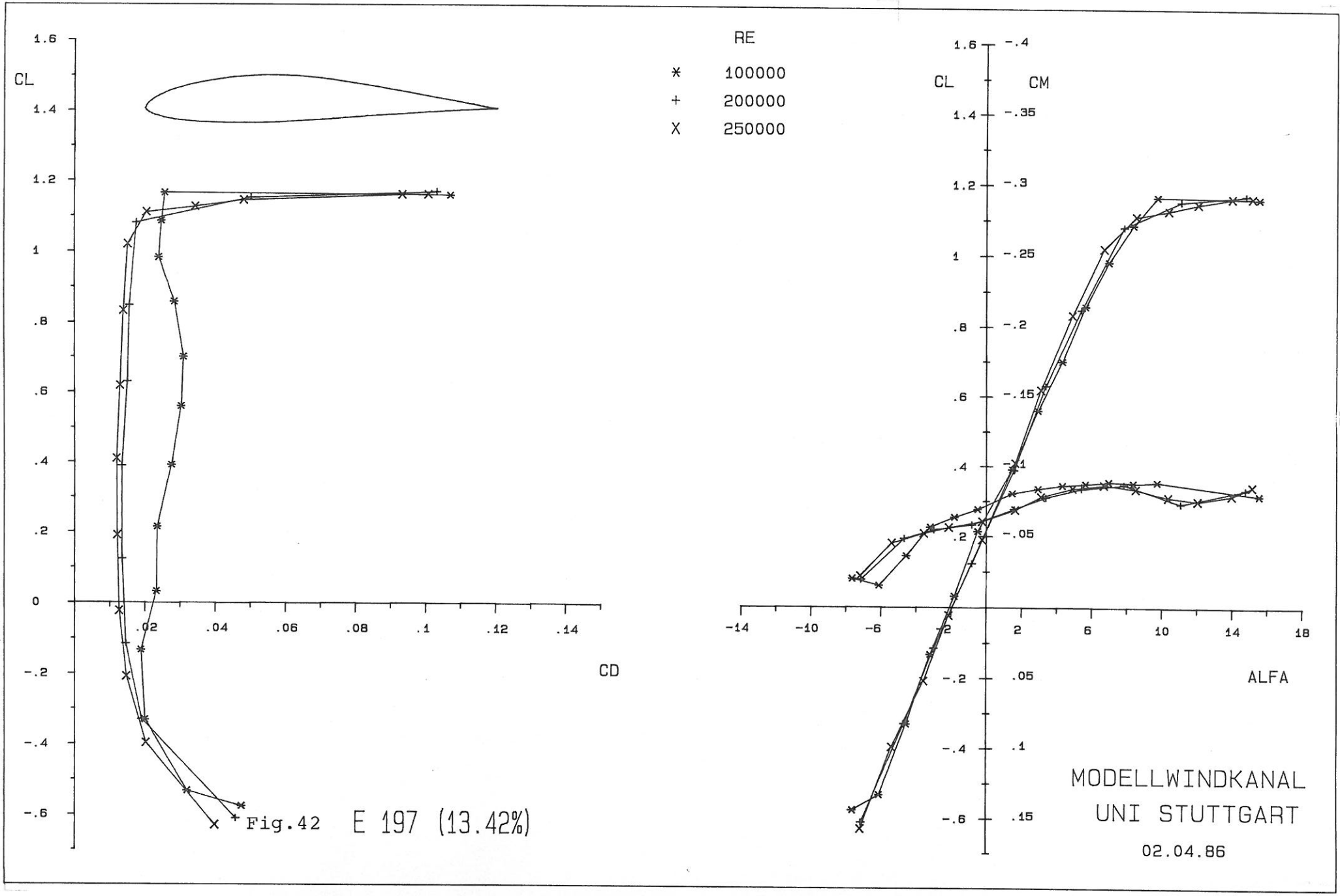

Fig.42 E 197 (13.42%)

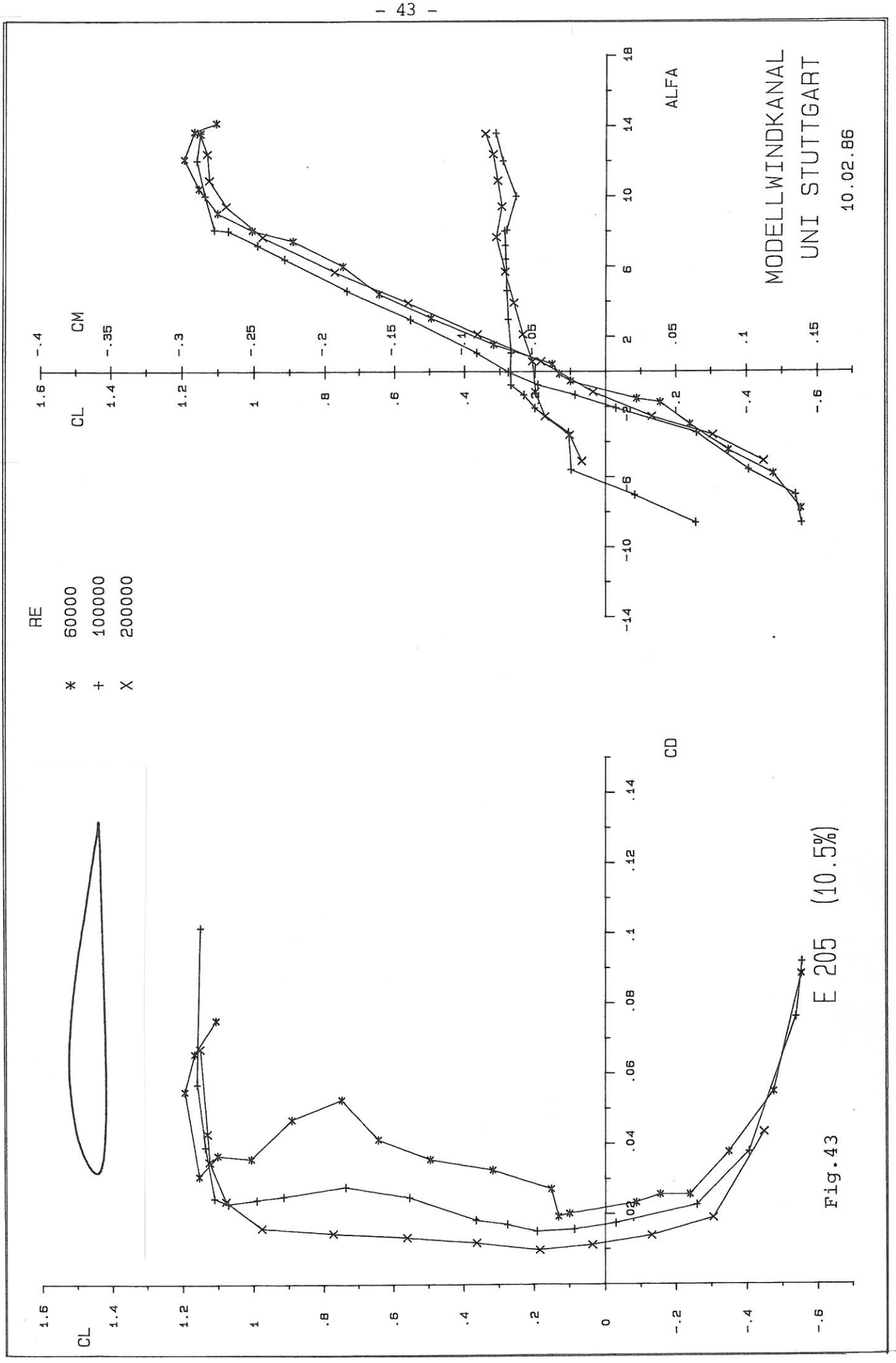
MODELLWINDKANAL
UNI STUTTGART
10.02.86
E 205 (10.5%)
RE
* 60000
+ 100000
X 200000
CL
CM
CD
ALFA

Fig.43

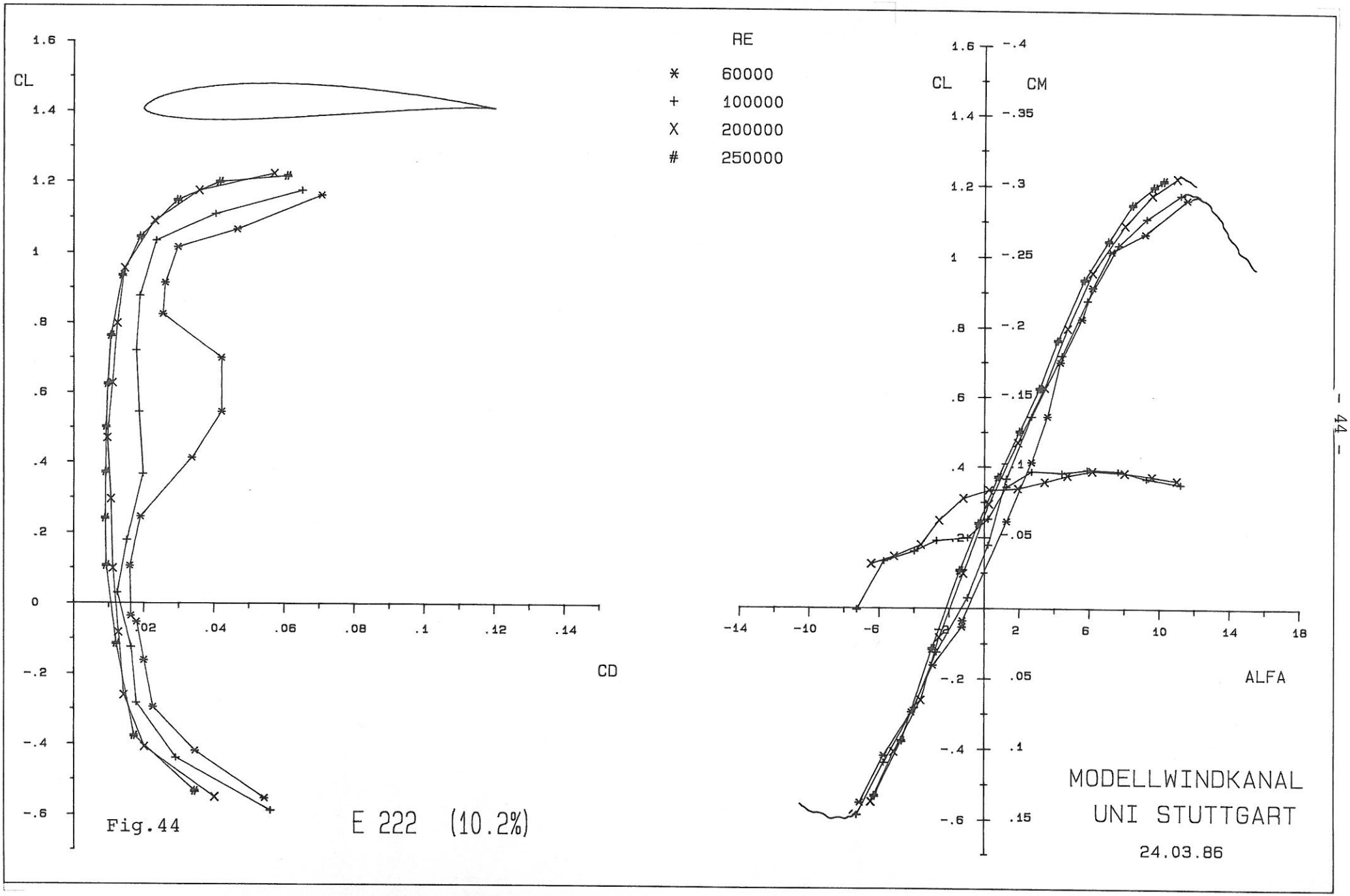

Fig.44 E 222 (10.2%)

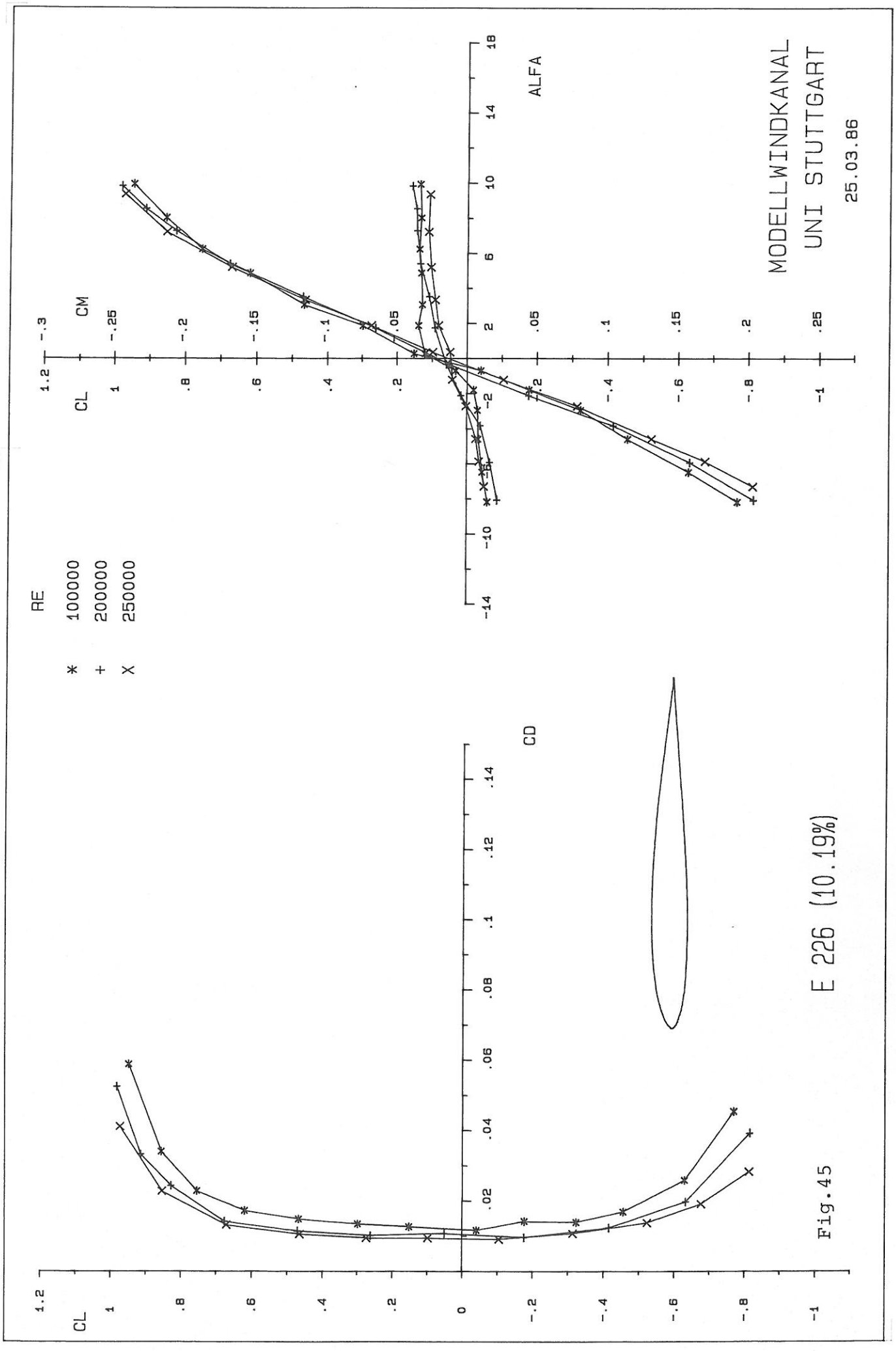
MODELLWINDKANAL
UNI STUTTGART
25.03.86
RE
* 100000
+ 200000
X 250000
CL
CM
ALFA
CD
E 226 (10.19%)

Fig.45

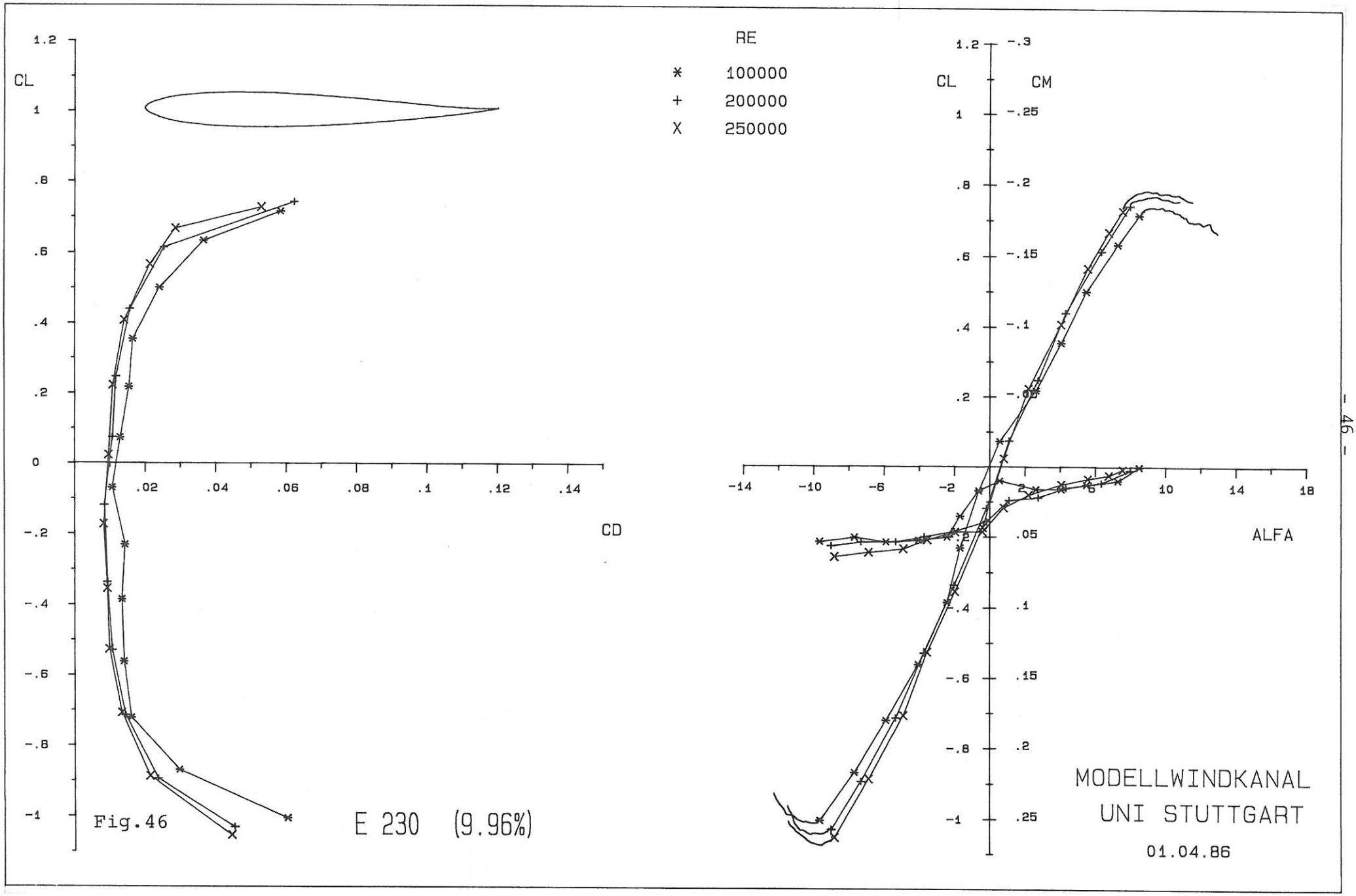

Fig.46 E 230 (9.96%)